Seasonal variations of ultrafine and sub-micron aerosols in Taipei, Taiwan: implications for particle formation processes in urban areas

Cheung, H. C.[1], Chou, C. C.-K.[1,*], Chen, M.-J.[1], Huang, W.-R.[1], Huang, S.-H.[1], Tsai, C.-Y.[1], Lee, C. S. L.[2]

1. Research Center for Environmental Changes, Academia Sinica, Taipei 11529, Taiwan
2. Institute of Occupational Medicine and Industrial Hygiene, College of Public Health, National Taiwan University, Taipei, Taiwan

**Correspondence to*: C. C.-K. Chou (ckchou@rcec.sinica.edu.tw)

Abstract

The aim of this study is to investigate the seasonal variations in the physicochemical properties of atmospheric ultrafine particles (UFPs, d ≤ 100nm) and submicron particles (PM_1, d ≤ 1μm) in an East-Asian urban area, which are hypothesized to be affected by the interchange of summer and winter monsoons. An observation experiment was conducted at the TARO (Taipei Aerosol and Radiation Observatory), an urban aerosol station in Taipei, Taiwan, from October 2012 to August 2013. The measurements included the mass concentration and chemical composition of UFPs and PM_1, as well as the particle number concentration (PNC) and number size distribution (PSD) with size range of 4-736 nm. The results indicated that the mass concentration of PM_1 was elevated during cold seasons with a peak level of 18.5 μg m^{-3} in spring, whereas the highest UFPs concentration was measured in summertime with a mean of 1.64 μg m^{-3}. Moreover, chemical analysis revealed that the UFPs and PM_1 were characterized by distinct composition; UFPs were composed mostly of organics, whereas ammonium and sulfate were the major constituents in PM_1. The seasonal median of total PNCs ranged from 13.9×10^3 cm^{-3} in autumn to 19.4×10^3 cm^{-3} in spring. Median concentrations for different size distribution modes peaked in different seasons. The nucleation mode PNC ($N_{4\text{-}25}$) peaked at 11.6×10^3 cm^{-3} in winter, whereas the Aitken mode ($N_{25\text{-}100}$) and accumulation mode ($N_{100\text{-}736}$) exhibited summer maxima at 6.0×10^3 and 3.1×10^3 cm^{-3}, respectively. The change in PSD during summertime was attributed to the enhancement in the photochemical production of condensable organic matter that, in turn, contributed to the growth of aerosol particles in the atmosphere. In addition, clear photochemical production of particles was observed, mostly in summer season, which were characterized by averaged particle growth and formation rates of 4.0±1.1 nm h^{-1} and 1.4±0.8 cm^{-3} s^{-1}, respectively. The prevalence of new particle formation (NPF) in summer was

suggested as a result of seasonally enhanced photochemical oxidation of SO_2 that contributed to the production of H_2SO_4, and low level of PM_{10} ($d \leq 10\mu m$) that served as the condensation sink. Regarding the sources of aerosol particles, correlation analysis upon the PNCs against NO_x revealed that the local vehicular exhaust was the dominant contributor of the UFPs throughout the year. On the contrary, the Asian pollution outbreaks had significant influence in the PNC of accumulation mode particles during the seasons of winter monsoons. The results of this study implied the significance of secondary organic aerosols in the seasonal variations of UFPs and the influences of continental pollution outbreaks in the downwind areas of Asian outflows.

1. Introduction

Due to the significant impact of particulate matter on human health and climate change, it is vital to understand the formation process of atmospheric particles (Charlson et al., 1992; Donaldson et al., 1998). A number of mechanisms have been proposed by which atmospheric particles are formed, including binary nucleation, ternary nucleation and ion-induced nucleation for charged particles, under different environment conditions (Kulmala 2003; Kulmala et al., 2004, 2012). Numerous studies have been conducted in different locations to elucidate particle formation processes under various environmental settings in the free troposphere, boreal forest and coastal areas, where new particles formation processes are observed frequently (Kulmala et al., 2004, Holmes 2007). Recently, investigations were also carried out on new particle formation within urban boundary layer (e.g., Cheung et al., 2013 and references therein), where particle formation was suggested to be mainly influenced by the photo-oxidation of SO_2. Furthermore, formation of particulate matter by heterogeneous reactions of gases on dust particles was reported recently (Hsu et al., 2014, Nie et al., 2014). Previous investigations have indicated that the air pollutants, both in gaseous and particulate form, associated with the continental outflows of air masses could have affected a wide region in East Asia and caused severe regional air pollution (e.g., Lin et al., 2004; Wang et al., 2003; Buzorius et al., 2004). However, the formation processes of ultrafine particles (UFPs, $d \leq 100$nm) and sub-micron particles (PM_1, $d \leq 1\mu m$) under the influences of continental outflows are not yet well understood.

In urban environment, major contributing sources of aerosol particles include vehicular exhausts (e.g., Pey et al., 2008; Pérez et al., 2010), industrial emissions (Gao et al., 2009) and new particle formation by photochemical reactions (e.g., Pey et al., 2009). Approximately 55-69% of the total particle number concentrations (PNCs) were attributed to secondary aerosols during midday in several European cities (Reche et al., 2011). In Taipei, Taiwan, a subtropical urban area, Cheung et al. (2013) observed that there was a ten-fold increase in nucleation mode particle number concentration ($N_{9\text{-}25}$, with size $9 < d < 25$nm) during new particle formation events compared to that contributed by the vehicle emission. Besides the local sources, air quality of East Asian countries is also strongly affected by the transport of air pollutants from mainland China during periods of winter monsoons (Cheung et al., 2005; Lin et al., 2004; Matsumoto et al., 2003). Lin et al. (2004) reported that the mass concentration of particulate matter (PM_{10}) due to the long-range transport associated with winter monsoons was 85 $\mu g\ m^{-3}$, about 79% higher than that due to local pollution (~47.4$\mu g\ m^{-3}$) in urban Taipei. Chemical composition of fine and

coarse particles was measured during a winter monsoon period at Rishiri Island, near the northern tip of Japan, to study the transport of continental aerosols (Matsumoto et al., 2003). The results showed that higher levels of particle mass concentrations were associated with the outbreaks of continental polluted air masses. In addition, Cheung et al. (2005) found deterioration in visibility around the southern China during wintertime as indicated by a two-fold increase in aerosol light scattering coefficient under the influences of winter monsoons. Chen et al. (2013) conducted a measurement of the particle number concentration at the background station on the mountain of central Taiwan in summer 2009 and autumn 2010. The result showed that particle number concentrations were dominated by local sources rather than long-range transport due to the short lifetime of nano-particles. Most of the previous studies mentioned above were limited to measurements in terms of PM_{10} or $PM_{2.5}$ for a particular period. However, the seasonal variations of particles in either ultrafine or sub-micron range have not been well illustrated.

A 1-year aerosol characterization experiment was conducted in the urban area of Taipei, Taiwan. The aim of this study is to attain a better understanding of the seasonal variations of ultrafine and sub-micron particles and the factors affecting particle formation, particularly under the influences of Asian monsoon circulations. In this study, we analyzed number concentration and size distribution of aerosol particles, together with the mass concentration and chemical composition of UFPs and PM_1 measured during four seasonal campaigns (i.e. 24 Oct – 15 Nov 2012, 4 – 24 Jan, 17 Mar – 11 Apr, and 1 – 14 Aug 2013). The results of this study will contribute to the management strategies of the severe air pollution over the East Asia region.

2. Methodology

2.1 Observation site and instrumentation

The measurements were conducted at the Taipei Aerosol and Radiation Observatory (TARO, 25.02 N, 121.53 E), located in the downtown area of Taipei, Taiwan, during October 2012 to August 2013. The measurements were carried out for 2 – 3 weeks in each season (see **Table 1** for measurement details). The aerosol observatory locates on the top floor of the Building-B of the Department of Atmospheric Sciences, National Taiwan University (ASNTU), which is ~20 m above ground level (Cheung et al., 2013).

Particle number size distribution (PSD) in the range of 4 – 736 nm was measured by two scanning mobility particle sizer (SMPS) systems. One was equipped with a long-differential mobility analyzer (long-DMA, Model: TSI 3081, TSI Inc.) and a

condensation particle counter (CPC) (Model: TSI 3022A, TSI Inc.) to measure the particles from 10 – 736 nm, which was named long-SMPS. Another one was equipped with a nano-DMA (Model: TSI 3085, TSI Inc.) and an ultrafine water-based CPC (UWCPC, Model: TSI 3786, TSI Inc.) to measure the particles from 4 – 110 nm, which was named nano-SMPS. The poly-disperse particles were classified into selected mono-disperse particles according to their electrical equivalent mobility by the DMAs. The number concentration of the mono-disperse particles was then counted by the CPCs. Ambient air was drawn into the SMPS systems from outside the building through a 0.635 cm (inner diameter) conductive tube, and a sampling duration of 5 min was adopted for each PSD measurement. The SMPS systems' flow rates were checked weekly during the sampling period and the accuracy of the particle sizing of the DMAs was checked using polystyrene latex (PSL) spheres before the campaigns. Operation details are referred to Cheung et al. (2013).

Size segregated aerosol samples were collected by a pair of Micro-Orifice Uniform Deposition Impactors (MOUDI, Model: 110, MSP Corp.). Taking the advantage that the cut diameter of the 9th MOUDI impaction stage was exactly 100 nm, the 10th impaction stage (cut diameter = 56 nm) of each MOUDI was removed to allow the after filter function as a collector of UFPs (Marple et al., 1991). The sampling flow rate of MOUDI sampler was 30 lpm. Besides, a pair of PM_1 samplers, each consisted of a standard aerosol sampler (PQ-200, BGI Inc.) and a PM_1 sharp cut cyclone, were deployed to collect PM_1 samples with 16.7 lpm sampling flow rate. For both UFPs and PM_1 sampling arrangements, one of the paired samplers was equipped with Teflon filters, whereas another was equipped with quartz fiber filters. The Teflon filter samples were used for gravimetric measurement. The quartz filter samples were deployed for analysis of soluble ions (Na^+, NH_4^+, K^+, Ca^{2+}, Mg^{2+}, Cl^-, NO_2^-,NO_3^-, SO_4^{2-}) using ion chromatograph (IC), and carbonaceous components (i.e. organic carbon, OC and elemental carbon, EC) in the aerosols using a DRI-2001A carbonaceous aerosol analyzer with IMPROVE-A protocol (Chow et al., 2007). Details of the in-lab analysis are as described previously (Salvador and Chou, 2014). Both the PM_1 and UFPs were collected with double-layered quartz filters (i.e. QBQ setup) and the artifacts due to adsorption of gaseous components were corrected as suggested by Subramanian et al. (2004). The sampling duration of each sample set (for both MOUDI and PQ-200 samplers) was from 14:00 - 12:00 LT (22 hr), and a total of 69 and 75 sets of UFPs and PM_1 samples were collected during the entire investigation period (sample sets collected in autumn, winter, spring and summer were 20, 15, 25, and 9 sets for UFPs, and 21, 16, 25, and 13 sets for PM_1, respectively).

Moreover, to assist the data interpretation, the hourly averaged mass concentration of PM_{10}, the mixing ratio of trace gases (i.e. NO_x, SO_2 and O_3) and the meteorology parameters (i.e. wind direction/speed and UVB (wavelength: 280 - 315 nm)) from the Guting air quality station of Taiwan Environmental Protection Agency, which is about 1 km from the TARO, were analyzed in this study. The details of instrumentation setup for trace gas measurements are referred to Cheung et al. (2013).

2.2 Data processing and analysis

The PSD of 4 – 736 nm presented in this study was combined from two sets of SMPS data, where the nano-SMPS corresponded to the size range of 4 – 50 nm, and the long-SMPS corresponded to the size > 50 nm. The diffusion loss of the particles during the sample transport in the tubing was corrected according to the algorithm proposed by Holman (1972). Particle number concentrations for different size ranges were then calculated from the SMPS measurements.

The 5-min PSD data were synchronized into hourly averages, and fitted by the DO-FIT model developed by Hussein et al. (2005) according to the multiple log-normal distribution algorithms. Based on the fitted PSD data, the PNCs were classified into $4 \leq d \leq 25$ nm ($N_{4\text{-}25}$), $25 < d \leq 100$ nm ($N_{25\text{-}100}$), $4 \leq d \leq 100$ nm ($N_{4\text{-}100}$), $100 < d \leq 736$ nm ($N_{100\text{-}736}$) and $4 \leq d \leq 736$ nm ($N_{4\text{-}736}$), for nucleation mode, Aitken mode, ultrafine, accumulation mode and total particles, respectively. Pearson correlation coefficient, *r*, was calculated by *PASW Statistics ver. 18* (SPSS Inc.) to determine the correlation between the respective parameters.

2.3 Classification of new particle formation and calculation of the particle growth and formation rates

A NPF event is defined as the increase of the number concentration of nucleation mode particles, where those particles are growing into Aitken and/or accumulation mode size range (≥ 25 nm) and last for a few hours until they coagulate on the pre-existing aerosol and/or other surfaces in the atmosphere. The calculation of particle growth rate (*GR*) was represented by the rate of geometric median diameter (*GMD*) changes during the period of nucleation mode particles growing through 25 nm (Cheung et al., 2013). The formation rate (*J*) of nucleation mode particles for each NPF event was calculated for the particle size ranging from 4-25 nm according to the method of Dal Maso et al. (2005). The formation rate is defined as the sum of the apparent formation rate ($dN_{4\text{-}25}/dt$) and the coagulation loss rate during the NPF event. It should be noted that the reported apparent particle formation rate is expected to be smaller than the actual nucleation rate, since some fraction of formed nuclei are

always scavenged by coagulation into larger pre-existing particles before they grow larger by condensation (Lehtinen et al., 2007). The work done by Kulmala et al. (2012) was referred for overview of the methodology on the measurement of the nucleation of atmospheric particles.

2.4 Back-trajectory analysis

Backward trajectories were calculated using the HYSPLIT model (Hybrid Single Particle Lagrangian Integrated Trajectory, Version 4.9) of NOAA (National Oceanic and Atmospheric Administration) (Draxler, 1999) for TARO during the sampling period, in order to trace the origins of the air masses. 72-h back trajectories were calculated twice per day at 00:00LT and 12:00LT with height setting of 200 m above ground level. It should be noted that the grid resolution of the meteorological data used for back-trajectories calculation is 1° x 1°, which is not enough to trace the detailed air mass passage over the scale of the study region and, therefore, the trajectories only provide an indication of the region from which the air mass was originated.

3. *Results and discussions*

3.1 Particle number concentration and size distribution in respective seasons

As mentioned above, the air quality of urban Taipei is significantly affected by both the local vehicular exhausts and long-range transport of pollution, where the later is dominated by meteorological factors. The information on the meteorological conditions, particularly the wind patterns, is important to elucidate our results and thus presented here. The back-trajectories of the air masses for the TARO are illustrated in **Figure 1 (left panel)**. The results showed that northeasterly winds prevailed in autumn and winter seasons, passing through the Asian continent before reaching Taiwan, whereas southerly winds prevailed in summertime. The air masses observed in spring period were found to be mainly associated with Asian continental outflows and occasionally with the southerly flows. This observation agreed with the surface wind direction measured in urban Taipei area (see **Figure 1, right panel**), where northeasterly winds were dominating during the period from November 2012 to May 2013, and southerly winds were prevailing from May 2013 to August 2013.

The particle number concentrations in various size ranges during each season are summarized in **Table 1**. Relatively higher total PNCs ($N_{4\text{-}736}$) were observed in spring and winter with median values of 19.4×10^3 and 17.4×10^3 cm^{-3}, respectively, followed by that of summer (16.6×10^3 cm^{-3}) and autumn (13.9×10^3 cm^{-3}). This result is comparable to the previous measurements conducted in urban Taipei where the

seasonal means of PNCs ($10 < d < 560$nm) ranged from $11.0x10^3$ to $17.0x10^3$ cm^{-3} (Cheng et al. 2014). **Figure 2** illustrates the number, surface and volume size distributions of the aerosol particles. The geometric mean diameter (GMD) of each PSD mode was retrieved from the data of number concentration. The GMDs of the nucleation, Aitken and accumulation modes were found to be 10.4-12.8 nm, 26.5-38.4 nm, and 91.8-159.0 nm, respectively. Details of particle number concentration and GMDs of each fitted mode in four seasons were listed in **Table S1** of appendix.

In addition, the fitted GMDs of surface distribution were found to be 77.4 and 293 nm for autumn, 22.1, 68.9 and 228 nm for winter, 77.4 and 253 nm for spring, and 12.9 and 268 nm for summer, respectively (not shown in the figures). In winter and summer seasons, one of the fitted surface GMDs was located at nucleation mode, showing the significant contribution of nucleation mode particles in these two seasons. Bimodal volume distribution was obtained for all seasons where the fitted volume GMDs were 96.3 and 372 nm for autumn, 71.8 and 275 nm for winter, 99.5 and 339 nm for spring, and 99.5 and 237 nm for summer, respectively. The GMD of first volume mode was relatively stable in each season (i.e. 71.8-99.5 nm), but smaller GMD (237 nm) for the second volume mode was observed in summer. The results implied that a higher fraction of particles could have evolved from smaller size range (i.e. nucleation and Aitken modes) into accumulation mode, which coincided with our observation that NPF events occurred mostly in summer (see Section 3.4). Furthermore, this seasonal variability agrees with our previous findings that the growth rate of newly formed particles was correlated with the photolysis of ozone, an indicator of photochemical activity (Cheung et al., 2013). The causes responsible for the observed seasonal variations in PNCs will be detailed in the following sections. This was different from that observed in urban Beijing where relatively larger GMD was observed in accumulation mode due to the enhancement of condensation by higher photochemical activities in summer but without significant seasonal variations in Aitken mode distribution (Wu et al., 2008).

It was revealed that the nucleation mode particles were predominant in the PNCs during autumn, winter and spring in the study area, whereas a distinct size distribution pattern was observed in summertime. In summer, the fraction of nucleation (N_{4-25} / N_{4-736}) decreased to 0.44 (see **Table 1**) and the Aitken mode PNCs increased to be comparable to that of the nucleation mode, whereas the N_{4-25} / N_{4-736} ratios for other seasons ranged from 0.56 to 0.77 (see **Table 1**). Observation from another aspect is that the PNC of nucleation mode (N_{4-25}) peaked in winter and reached the minimum in summer, whereas the PNCs of Aitken mode (N_{25-100}) and accumulation mode ($N_{100-736}$)

reached their maxima in summertime. The changes in the size distribution in summer season were most likely due to the seasonally enhanced photochemical production of condensable vapors that, in turn, contributed to the growth of aerosol particles in the atmosphere.

3.2 Mass concentration and chemical composition

Figures 3a and **3b** illustrate the averaged chemical composition and mass concentration of UFPs and PM_1, respectively, for each season. Details of the mass concentration and chemical composition of UFPs and PM_1 are listed in Table S2 in the appendix.

The seasonal means of UFPs ranged from 0.73 to 1.64 μg m^{-3}, with an annual average of 1.01 μg m^{-3}. The measured UFPs mass concentration of the present study was comparable to that in urban area of Los Angeles, United States (0.80 – 1.58 μg m^{-3}, Hughes et al. 1998), and relatively higher than that in urban Helsinki, Finland (average: 0.49 μg m^{-3}, Pakkanen et al. 2001). For the chemical composition, OC was found to be the major mass contributor, which accounted for 29.8 % (seasonal means ranging from 26.9 to 33.4 % for various seasons) of averaged mass concentration of UFPs. The EC was the second major component with averaged mass contribution of 5.1 % (seasonal means: 2.4–7.6 %), followed by sulfate (SO_4^{2-}) at 4.3 % (seasonal means: 3.4-6.4%) and nitrite (NO_2^-) at 2.9% (seasonal means: 0.9-7.3%). In addition, a large fraction of mass was contributed by the group of "others", which consisted of mineral (K^+, Ca^{2+}, PO_4^{3-} and Mg^{2+}), sea-salt (Na^+ and Cl^-), and unidentified species. The results showed that, on average, mineral and sea salt components attributed only 3.5 % (seasonal means: 2.0-6.0 %) to UFPs mass concentration. Thus a substantial amount of UFPs remained unidentified, which likely included hydrogen and oxygen associated with OC. The conversion factors used to estimate the average molecular weight per carbon in particulate organic matter varied depending on the characteristic of aerosols. A lower factor value, 1.2, was usually suggested for saturated organic molecules, while a higher value, 1.6, was adopted for water-soluble compounds consisting of multifunctional oxygenated groups, and even higher factor values were suggested for aged aerosols which contained higher portion of low and semi-volatile products of photochemical reactions (Turpin and Lim et al. 2001). The high un-identified mass fraction implied that the photochemical production of secondary organic aerosols was a significant process responsible for the elevated UFPs levels observed in this study.

As shown in Fig. 3b, average PM_1 was estimated to be 14.7 μg m^{-3} (seasonal

means: 11.6-18.5 μg m^{-3}) in this study, which is similar to the results of a previous study in urban Taipei (average: 14.0 μg m^{-3}, Li et al., 2010). The measured PM_1 level is relatively higher than that of the urban areas of Phoenix, United States (5.9 μg m^{-3}, Lundgren et al. 1996) and Helsinki, Finland (6.1 μg m^{-3}, Vallius et al. 2000). For chemical composition, sulfate was the major mass contributor of PM_1 (average: 39.0 %, seasonal means: 33.8 - 46.8 %), followed by ammonium (average: 12.7 %, seasonal means: 12.0 - 13.2 %) and OC (average: 11.5 %, seasonal means: 9.2 to 14.3 %).

The results presented above indicated that UFPs exhibited a distinct seasonal variability and composition from PM_1 in the study area. The highest UFPs concentration was observed in summer (1.64 μg m^{-3}) and the lowest in winter (0.73 μg m^{-3}). This result may be attributed to the stronger photochemical activities in summer which could have enhanced the formation of secondary organic aerosols. Consequently, the mass concentration of OC increased from 0.20 μg m^{-3} in winter to 0.47 μg m^{-3} in summertime. It is noteworthy that the mass concentration of sulfate in UFPs also peaked in summer (64 ng m^{-3}), suggesting enhancement in photo-oxidation of SO_2. Cheung et al. (2013) found that photo-oxidation of SO_2 was the major mechanism for the formation of new particles in Taipei, Taiwan and the production of condensable vapors was also dominated by photo-oxidation. The co-variations in sulfate and OC revealed in this study further suggested that secondary organic compounds were the major condensable matter contributing to the growth of newly formed particles.

While the organics predominated in the mass concentration of UFPs, which included nucleation mode and Aitken mode particles, the measurements of PM_1 in this study suggested that sulfate was the major constituent of accumulation mode aerosols. In contrast to the seasonal variation of UFPs, the mass concentration of PM_1 reached the maximum at 18.5 μg m^{-3} in spring and exhibited the minimum at 11.6 μg m^{-3} in summer. The PM_1 differences between spring and summer were mostly due to declined ambient levels of sulfate, nitrate, and ammonium ions. As a result, the mass contribution of the three inorganic ions in PM_1 reduced from 55.7 % to 46.2 % and, on the contrary, the mass fraction of OC increased from 10.2 to 14.3 %. The seasonal characteristics of PM_1 concentration and composition were attributed mostly to the changes in the origin areas of background air mass, which shifted from the Asia Continent to the western Pacific Ocean during summertime (see **Fig. 1**). Our previous studies reported that the fine particulate matter ($PM_{2.5}$) transported on the Asian outflows to northern Taiwan maximized in springtime and were enriched in sulfate,

nitrate, and ammonium (Chou et al., 2008; 2010). The seasonal variability of PM_1 found in this study was consistent with the previous observations for $PM_{2.5}$ and thereby suggested the significance of Asian outflow aerosols to the PM_1 budget in the downwind areas of the Asia Continent.

3.3 Seasonal characteristics of photochemical production

In order to study the influences of photochemical production of particles, the measurements of PNC and PSD were analyzed per daytime (07:00 – 17:00 LT) and nighttime (17:00 – 07:00 LT), respectively (see **Figure 4**). In urban environment, the possible sources influencing the PNC and PSD are complicated, which include not only the direct emission from primary sources but also interaction between the newly formed particles, pre-existing particles and condensing vapors through the condensation and coagulation processes. Nevertheless, these processes occurred throughout the day and will not dominate in the differences between daytime and nighttime PNCs as observed in this study. It was assumed that photochemical reaction was the major attributing factor to the observed diurnal differences in PNC. Since the particles in nighttime were mainly emitted from the vehicular exhausts and the elevated PNCs in daytime were due to both the primary and secondary sources of the particles in the study area (Cheung et al., 2013), a larger difference between the PNCs observed in daytime and nighttime indicated stronger influences of photochemical production on the PNCs. The most striking seasonal features shown in **Figure 4** is the large difference between daytime against nighttime PSD in summer as indicated by the low $N_{4\text{-}736}$ (nighttime)/$N_{4\text{-}736}$ (daytime) ratio, whereas higher ratios were observed in other seasons. In addition, the diurnal variation of particle size distribution (see **Figure 5**) provided further information about the variations in PSD. Two nucleation bursts were distinctly observed in morning and afternoon traffic peak hours in autumn, winter, and spring, while a typical PSD pattern of nucleation event (increase of nucleation mode particle concentrations with subsequent growth in particle size) was dominant in summer. This result is as expected because the photochemical production of nucleation mode particles is more intense during warm seasons (Cheung et al., 2011). Moreover, as discussed in previous section, the photochemical reactions could produce condensable organics that allows the newly formed nucleation mode particles to grow into the Aitken mode. The relatively small differences between the daytime and nighttime $N_{4\text{-}736}$ in autumn and winter indicated that the photochemical contribution in PNCs was declined as compared to that in summertime. Nevertheless, the contribution of vehicle emission was also significant, especially during colder seasons and when photochemical reactions were less intense. This will be discussed in detail in Section 3.5.

3.4 Factors affecting new particle formation (NPF)

As shown in previous study, the NPF events were frequently observed in summer, which subsequently induced a notable increase in N_{4-25} in urban Taipei (Cheung et al. 2013). The frequency of NPF events was found to be 10 out of 84 measurement days and the events were observed in autumn (1 out 23 days), spring (3 out of 26 days) and summer (6 out of 14 days) seasons. **Figure 6** (a-d) shows the scatter plots of N_{4-25} against NO_x for daytimes in each season. During the NPF events, a non-linear relationship between these two parameters was usually observed during the daytime (Cheung et al. 2013). The results showed that clear NPF events were observed often in summer and occasionally in spring, but rarely in autumn and winter in the study area. The averaged particle growth and formation rates were found to be 4.0±1.1 nm h^{-1} and 1.4±0.8 cm^{-3} s^{-1}, which were comparable to those measured in other urban studies in Asian cities such as Hong Kong (average: 6.7 nm h^{-1}, Wang et al., 2014) and Beijing (average: 5.2 nm h^{-1}, Wang et al., 2013) , and also within the range observed in other nucleation studies across the globe (~1 - 20 nm h^{-1}, Kulmala et al., 2004). The particle growth and formation rates of each case are listed in **Table 2**.

Table 3 summarizes the averages of N_{4-25}, PM_{10}, H_2SO_4 proxy (as UVB*SO_2/condensation sink) and wind speed for each season. Petäjä et al. (2009) calculated the H_2SO_4 proxy with a pre-factor value, *k*, and use it to estimate the actual sulfuric acid concentration. The estimation of a site-specific *k* value requires an actual measurement of H_2SO_4 which is not available in this study area. The proxy value calculated in this study was therefore only used as an indicator of particle production strength contributed by H_2SO_4. The dominating factors associated to the frequent particle formation in summertime were the low PM_{10} concentration (35.6 μg m^{-3}) and high H_2SO_4 proxy (493.1 ppb W m^{-2} s). The association of sulfuric acid production and the NPF events agreed with the elevated mass concentration of sulfate in UFPs during summertime (shown in **Table S2**), as well as the results of previous urban studies (Woo et al. 2001; Cheung et al. 2013). This strongly suggested that the new particle formation was mainly driven by the photochemical oxidation of SO_2 under low condensation sink conditions (Gao et al., 2009; Nie et al., 2014), where the SO_2 could be transported from the upwind area on the summer monsoons (see **Figure 1d**). Contrarily, the absence of particle formation events in wintertime could be attributed to the declined photochemical production of H_2SO_4 as well as suppression of NPF by particles transported from the Asian continent (Lin et al., 2004). The results of this work evidenced that low PM_{10} concentration and high sulfuric acid production favored the particle formation process in urban areas. Nevertheless, it should be noted that condensing vapors other than sulfuric acid, for example VOCs, could also

contribute to the observed particle formation, which requires further investigation.

The scatter plot between UVB*SO_2 and condensation sink is depicted in **Figure 7**. Relatively higher UVB*SO_2 values were obtained during NPF events. Notably, there was a group of data with high UVB*SO_2/CS but low UVB*SO_2 where no NPF event was observed. This implied that there could be a threshold level of UVB*SO_2 for NPF in the study region. However, some exceptions existed in the dataset and suggested that the parameters driving NPF have not been well accounted and need to be further studied. It was also noticed that an Asian outflow event occurred on 7 April 2013 during which an atypical NPF was observed (labeled as black dot in **Figure 7**). This could be relevant to the secondary particle formation on dust surface under the influence of long-range transport of air mass. This will be discussed in further details in Section 3.6.

3.5 Influences of local emission on PNCs

Vehicle emission is known as the major source of the particulate matter in urban environment, particularly during the nighttime. In order to investigate the relationship between the vehicular exhausts and PNCs, the scatter plots of NO_x (as an indicator of vehicle emission) against $N_{4\text{-}25}$, $N_{25\text{-}100}$ and $N_{100\text{-}736}$ during the nighttime were examined for winter and summer periods (see **Figure 8**). The values of the Pearson correlation coefficient (r) and the slope of linear regression between NO_x and PNCs are summarized in **Table 4**.

The highest r values were found in both the plots of NO_x against $N_{25\text{-}100}$ for winter (r = 0.88) and summer (r = 0.87). This result suggested a strong linear correlation between the vehicle emission and the $N_{25\text{-}100}$ which coincided with the results from previous studies (e.g., Morawska et al. 2008). During wintertime, stronger correlation was found between NO_x against $N_{4\text{-}25}$ (r = 0.84) and $N_{25\text{-}100}$ (r = 0.88) compared to that between NO_x and $N_{100\text{-}736}$ (r = 0.38). In contrast, high r values were obtained between NO_x and all particle modes in summer (r = 0.70 - 0.87). The robust correlation of NO_x and $N_{4\text{-}25}$, also NO_x and $N_{25\text{-}100}$ suggested that local vehicle emission was the predominant source of UFPs throughout a year. These results coincided with previous studies on the size distribution of vehicle exhaust particles, which were found to be 20-130 nm and 20-60 nm, respectively, for diesel and petrol engine vehicles (Harris and Maricq 2001, Ristovski et al. 2006). However, the PNCs of accumulation mode particles ($N_{100\text{-}736}$) in winter were dominated by NO_x-independent sources, which were most likely related to the pollution outbreaks from the Asian continent. Lin et al. (2004) indicated that the long-range transported air mass was characterized by high level of PM_{10} and low mixing ratio of NO_x due to

its short atmospheric lifetime. Interestingly, a moderate correlation between the PNC of accumulation mode particles ($N_{100-736}$) and NO_x was also observed in summer. Given that the Asian outflow was ceased in summertime, this correlation evidenced substantial contribution of local sources, particularly vehicular emissions, to the PNC of accumulation mode particles in Taipei, Taiwan.

The slope values can serve as a relative emission factor of particles per NO_x, which indicates the degree of influence of vehicle emission on the PNCs (Cheung et al., 2013). The corresponding slope values for N_{4-25}, N_{25-100}, and $N_{100-736}$, were found to be 279, 163, 18 $cm^{-3} \cdot ppb^{-1}$ in winter, and 239, 330, 155 $cm^{-3} \cdot ppb^{-1}$ in summer. Larger sum of slope values (724 vs. 460 $cm^{-3} \cdot ppb^{-1}$) was found in summertime compared to winter period, evidencing a greater influence of the vehicle emission on particle number concentration. The seasonal effects on the emission ratio of PNCs and NO_x are rather difficult to address due to the complexity of different controlling factors, such as formation mechanisms and meteorological conditions. For example, Nam et al. (2010) reported negatively exponential correlation between the PM/NO_x ratio in vehicle emission and ambient temperature, and suggested that the impact of ambient temperature on particulate matter was larger than that on NO_x. Nevertheless, the observed differences in the $PNCs/NO_x$ ratios for winter and summer periods of this study necessitate further investigations on the formation mechanisms of aerosol particles in urban areas, in particular the nucleation and the Aitken modes.

3.6 Influence of long-range transport (LRT)

During the seasons of winter monsoons, i.e. from autumn to spring, the continental outflows have been frequently observed in urban Taipei, which is indicated by the stable northeasterly wind and increase of O_3 level (Lin et al. 2004). Previous studies of long-range transport (LRT) of air pollutants on air quality of northern Taiwan showed that an elevated PM_{10} was observed under the influence of continental outflows (Lin et al., 2004, Chou et al., 2004). **Figure 9** depicts an LRT pollution event observed at the TARO during this study. The wind direction changed from westerly/northwesterly to northeasterly at 21:00, 24 March which continued until 06:00, 26 March. During this period, the O_3 mixing ratio remained at moderate level (~30-55 ppb) and PM_{10} increased from 10.0 to 98.0 μg m^{-3}. It should be noted that the variations of measured pollutants were not solely influenced by the long-range transport, but also partly due to the variation of local pollution and boundary dynamics. In this section, we attempt to analyze the PSD/PNC under the influences of continental pollution outbreaks. The periods of the respective LRT events are listed in **Table S3**.

As shown in **Figure 9**, the diurnal variations of PSD during the LRT event exhibited two $N_{4\text{-}25}$ peaks associated to the morning and afternoon traffic rush hours, whereas the PNCs of the Aitken mode particles remained at a low level. The results suggested that the influences of local vehicle emission on PNCs were still in place, whereas growth of particles due to secondary production of condensable vapors could have been suppressed, as NPF was rarely observed during the LRT events. It is noteworthy that a weak dust transport event was observed on 7 April 2013 where a nucleation event was observed in the PSD, evidencing that secondary formation of particles could have had occurred. However, the dominating diameter of particles was ~ 40-50 nm at the initial stage of the event. The nucleation event initiated since ~06:00 LT until 21:00 LT, when the northeasterly wind prevailed. The PM_{10} and O_3 increased from minima of 44 μg m^{-3} (at 06:00 LT) and 25 ppb (at 05:00 LT) to the daily maxima of 92 μg m^{-3} (at 17:00 LT) and 61 ppb (at 16:00 LT). This result showed that the NPF process could have occurred in the upwind area where newly formed particles were transported to the study site, or heterogeneously formed particles were released from the dust surface during the long-range transport of air pollutants (Nie et al., 2014).

The averaged PSDs for LRT and non-LRT cases are shown in Figure 10. The GMDs of the nucleation, Aitken, and accumulation modes in PSD were found to be 10.4, 37.2 and 158 nm for LRT and 11.4, 30.4 and 114 nm for non-LRT cases, respectively (see Table S1 for detailed fit results of the PSD for LRT and non-LRT cases). The PNCs of different modes observed in non-LRT events were $8.6x10^3$ cm^{-3} (nucleation mode), $9.3x10^3$ cm^{-3} (Aitken mode) and $2.6x10^3$ cm^{-3} (accumulation mode). The PNCs of LRT events were $9.2x10^3$ cm^{-3} (nucleation mode), $4.0x10^3$ cm^{-3} (Aitken mode), and $1.3x10^3$ cm^{-3} (accumulation mode), respectively. The nucleation mode PNC observed in non-LRT was comparable with that in LRT events, whereas significant higher PNCs for the Aitken mode and accumulation mode were observed during non-LRT periods. This was attributed to the lower average wind speed (and hence poor dispersion) during non-LRT events (1.5±0.8 m s^{-1}) than that for LRT events (3.0±0.8 m s^{-1}). In contrast to the increase in PM_{10} observed usually during LRT episodes (e.g., Lin et al., 2012), the relatively lower PNCs suggested that the number concentration of submicron particles, in particular UFPs, was dominated by local emissions. This agreed with the observation of seasonal UFPs mass concentration that peaked in summertime when Taiwan was isolated from the influences of continental air mass.

4. Conclusions

The mass concentration and chemical composition of ultrafine particles (UFPs) and submicron particles (i.e. PM_1) as well as the particle number concentration (PNC) and size distributions (PSD) with size ranging from 4 to 736 nm were measured during four seasonal campaigns in the period from October 2012 to August 2013 at the TARO, a subtropical urban aerosol station in Taipei, Taiwan. Significant seasonal variability and chemical composition of UFPs and PM_1 were revealed. The UFPs were composed mostly of organic matter and reached maxima in summer, whereas the PM_1 composition was dominated by ammonium and sulfate and exhibited a seasonal peak in spring.

It was found that the total PNC was significantly elevated during cold seasons, which was caused mostly by the high level of nucleation mode particles ($N_{4\text{-}25}$). On the contrary, both the Aitken mode ($N_{25\text{-}100}$) and accumulation mode ($N_{100\text{-}736}$) PNCs reached their respective maxima in summertime. Consistent correlation without significant seasonal variations was found between the UFPs (i.e. nucleation and Aitken mode particles) and NO_x, suggesting that local vehicle emission was the major source of UFPs in the study area throughout a year. The local vehicle emission was also dominating the accumulation mode PNC in summer, but not in wintertime. The declined correlation between NO_x and $N_{100\text{-}736}$ in winter (r = 0.38) was likely due to the influences of air pollution associated with the Asian outflows.

The elevated UFPs level in summer was attributed to the increase in the concentration of Aitken mode particles ($N_{25\text{-}100}$). It was revealed from the measurements of PSD that a large number of nucleation mode particles could have evolved into the Aitken mode during summertime, which was most likely relevant to the photochemical production of condensable vapors that, in turn, could have contributed to the growth of particles in the atmosphere. Moreover, the chemical measurements suggested that the constituents of the condensed materials in UFPs were mostly organic matter, implying the significance of secondary organic aerosols in the ambient UFPs.

A total of 10 new particle formation (NPF) events occurred out of 84 measurement days in this study, which were observed in autumn (1 out 23 days), spring (3 out of 26 days) and summer (6 out of 14 days) seasons. The prevalence of NPF in summer agreed with the highest H_2SO_4 proxy and lowest PM_{10} observed in this study, which provided favorable atmospheric conditions for new particle formation. The averaged particle growth and formation rates for the NPF events were

582 4.0±1.1 nm h^{-1} and 1.4±0.8 cm^{-3} s^{-1}, respectively, which were comparable to those
583 measured in previous urban studies.
584
585 As exemplifying above, the characteristics of various physicochemical properties
586 of particles investigated in this study and the occurrence of NPF exhibited a strong
587 seasonal variability, which was co-influenced by the long-range transported particles
588 during the seasons of winter monsoons and the strong photochemical activities in
589 summer. The results of this study are critical for the authorities involved in urban
590 development and health impact assessment, and the environmental policy makers who
591 are tackling the severe atmospheric pollution in the East Asia region.
592
593 ***Acknowledgements***
594 This research was supported by the Academia Sinica and the Ministry of Science and
595 Technology of Taiwan through grants 103-2111-M-001-003, 102-2628-M-001-007,
596 and 101-2119-M-001-003. The authors thank the Taiwan EPA for providing the air
597 quality and meteorological data. We also thank the Department of Atmospheric
598 Science of National Taiwan University for the logistical supports to the operation of
599 TARO. Prof. Tareq Hussein is gratefully acknowledged for providing us the code of
600 DO-FIT.
601

602 **Table 1.** Median and quartile ranges (Q1-Q3) of the PNCs measured in each season. The size
603 ranges of the PNCs were represented by the subscripted number. For example, $N_{4\text{-}25}$,
604 represents the number concentrations of the particles from 4 to 25 nm. The fractions of $N_{4\text{-}25}$
605 and $N_{4\text{-}100}$ to total PNCs were presented in the last two columns.
606

	Measurement periods	$N_{4\text{-}736}$ (10^3 #/cm^3)	$N_{4\text{-}25}$ (10^3 #/cm^3)	$N_{25\text{-}100}$ (10^3 #/cm^3)	$N_{4\text{-}100}$ (10^3 #/cm^3)	$N_{100\text{-}736}$ (10^3 #/cm^3)	$N_{4\text{-}25}/N_{4\text{-}736}$	$N_{4\text{-}100}/N_{4\text{-}736}$
Autumn	24 Oct–15 Nov2012	13.9 (9.9–19.4)	8.6 (5.8–11.8)	3.9 (2.6-5.5)	12.7 (8.7-17.8)	1.3 (0.8-1.9)	0.62	0.90
Winter	4–24 Jan 2013	17.4 (12.7-22.3)	11.6 (8.2-15.1)	4.1 (2.8-5.6)	16.3 (11.6-21.4)	0.9 (0.5-1.5)	0.70	0.94
Spring	17 Mar–11 Apr 2013	19.4 (13.2-26.2)	10.3 (7.2-14.1)	5.8 (4.0-9.4)	17.0 (11.4-23.6)	1.9 (1.4-2.7)	0.56	0.89
Summer	1–14 Aug 2013	16.6 (9.2-26.7)	6.9 (4.5-10.4)	6.0 (2.5-11.3)	13.7 (7.9-21.4)	3.1 (0.5-5.1)	0.44	0.87

607

608 **Table 2.** Time periods defined as the new particle formation events and the particle growth
609 and formation rates

Date	*Time period (LT)*	*Growth rate (nm h^{-1})*	*Formation rate (cm^{-3} s^{-1})*
9 Nov 2012	07:00-13:00	3.4	1.30
26 Mar 2013	06:00-10:00	3.4	1.91
4 Apr 2013	07:00 – 10:00	3.7	1.13
5 Apr 2013	08:00 – 12:00	5.5	1.10
4 Aug 2013	09:00 – 12:00	3.9	1.84
5 Aug 2013	09:00 – 13:00	4.9	2.44
7 Aug 2013	06:00 – 12:00	3.5	0.84
8 Aug 2013	09:00 – 12:00	5.0	2.76
9 Aug 2013	06:00 – 13:00	1.6	0.39
11 Aug 2013	06:00 – 09:00	4.8	0.58
Average (±Standard Deviation)		4.0 (±1.1)	1.4 (±0.8)

610
611

Table 3. Average of N_{4-25}, PM_{10}, UVB, SO_2, condensation sink (CS), H_2SO_4 proxy and wind speed of different seasons. Standard deviation values shown in brackets (Note: the data with observation of rainfall was not used in calculation).

Periods	***N_{4-25} (10^3 #/cm^3)***	***PM_{10} (μg m^{-3})***	***UVB (Wm^{-2})***	***SO2 (ppb)***	***CS (10^{-2} s^{-1})***	***H_2SO_4 proxy (ppb Wm^{-2} s)***	***Wind speed (ms^{-1})***
Autumn	8.6 (±4.5)	53.9 (±21.4)	1.04 (±1.75)	2.27 (±1.44)	0.85 (±0.52)	307.1 (±609.1)	2.82 (±1.04)
Winter	11.6 (±9.2)	48.4 (±23.9)	0.80 (±1.47)	2.58 (±1.61)	0.75 (±0.61)	240.0 (±472.1)	2.34 (±0.89)
Spring	10.2 (±9.2)	61.1 (±27.0)	0.99 (±1.73)	2.76 (±1.67)	1.35 (±0.67)	238.4 (±533.6)	2.17 (±1.19)
Summer	6.9 (±9.1)	35.6 (±13.7)	1.97 (±2.95)	3.19 (±2.55)	1.89 (±1.51)	493.1 (±1066)	2.35 (±1.13)

Table 4. Pearson correlation coefficient (*r*) and slope of linear regression of PNCs against NO_x during the nighttime (20:00-04:00 LT) in winter and summer periods.

Periods		$N_{4\text{-}25}$	$N_{25\text{-}100}$	$N_{100\text{-}736}$
Winter	*Slope*	279	163	18
	r	0.84	0.88	0.38
Summer	*Slope*	239	330	155
	r	0.76	0.87	0.70

References

Buzorius, G., McNaughton, C.S., Clarke, A.D., Covert, D.S., Blomquist, B., Nielsen, K. and Brechtel, F.J. (2004). Secondary aerosol formation in continental outflow conditions during ACE-Asia. Journal of Geophysical Research, 109, doi:10.1029/2004JD004749.

Charlson, R.J., Schwartz, S.E., Hales, J.M., Cess, R.D., Coakley Jr., J.A., Hansen, J.E. and Hofmann, D.J. (1992). Climate forcing by anthropogenic aerosols. Science, 255, 423-430.

Chen, S.-C., Hsu, S.-C., Tsai, C.-J., Chou, Charles, C.-K., Lin, N.-H., Lee, C.-T., Roam, G.-D., Pui, D.Y.H. (2013). Dynamic variations of ultrafine, fine and coarse particles at the Lu-Lin background site in East Asia. Atmospheric Environment, 78, 154-162.

Cheng, Y.-H., Kao, Y.-Y. and Liu, J.-J. (2014). Correlations between black carbon mass and size-resolved particle number concentrations in the Taipei urban area: A five-year long-term observation. Atmospheric Pollution Research, 5, 62-72.

Cheung, H.C., Wang, T., Baumann, K. and Guo, H. (2005). Influence of regional pollution outflow on the concentrations of fine particulate matter and visibility in the coastal area of southern China. Atmospheric Environment, 39, 6463-6474.

Cheung, H.C., Morawska, L. and Ristovski, Z.D. (2011). Observation of new particle formation in subtropical urban environment. Atmospheric Chemistry and Physics, 11, 3823-3833.

Cheung, H.C., Chou, C.C.-K., Huang, W.-R. and Tsai, C.-Y. (2013). Characterization of ultrafine particle number concentration and new particle formation in an urban environment of Taipei, Taiwan. Atmospheric Chemistry and Physics, 13, 8935-8946.

Chou, C. C.-K., Lee, C. T., Cheng, M. T., Yuan, C. S., Chen, S. J., Wu, Y. L., Hsu, W. C., Lung, S. C., Hsu, S. C., Lin, C. Y., Liu, S. C. (2010). Seasonal variations and spatial distribution of carbonaceous aerosols in Taiwan, Atmos. Chem. Phys, 10, 9563–9578.

Chou, C. C.-K., Lee, C.-T., Yuan, C. S., Hsu, W. C., Hsu, S. C., Liu, S. C. (2008). Implications of the chemical transformation of Asian outflow aerosols for the long-range transport of inorganic nitrogen species. Atmospheric Environment, 42, 7508-7519.

Chou, C. C.-K., Huang, S.-H., Chen, T.-K., Lin, C.-Y. and Wang, L.-C. (2005). Size-segregated characterization of atmospheric aerosols in Taipei during Asian outflow episodes. Atmospheric Research, 75, 89-109.

Chou, C. C.-K., Lin, C.-Y., Chen, T.-K., Hsu, S.-C., Lung, S.-C., Liu, S.C. and Young, C.-Y. (2004). Influence of Long-Range Transport Dust Particles on Local Air Quality: A Case Study on Asian Dust Episodes in Taipei during the Spring of 2002.

Terrestrial, Atmospheric and Oceanic Sciences, 15, 881-889.
Chow, J. C., Watson, J. G., Chen, L.-W. A., Chang, L.C.O., Robinson, N. F., Trimble, D. and Kohl, S. (2007). The IMPROVE_A Temperature Protocol for Thermal/Optical Carbon Analysis: Maintaining Consistency with a Long-Term Database, Journal of the Air & Waste Management Association, 57:9, 1014-1023.
Dal Maso, M., Kulmala, M., Riipinen, I., Wagner, R., Hussein, T., Aalto, P.P. and Lehtinen, K.E.J. (2005). Formation and growth of fresh atmospheric aerosols: eight years of aerosol size distribution data from SMEAR II, Hyytiälä, Finland. Boreal Environ. Res., 10, 323-336.
Donaldson, K., Li, X.Y. and MacNee, W (1998). Ultrafine (nanometre) particle mediated lung injury. Journal of Aerosol Science, 29, 553, 560.
Draxler, R.R. (1999). HYSPLIT4 user's guide. NOAA Tech. Memo. ERL ARL-230, NOAA Air Resources Laboratory, Silver Spring, MD.
Gao, J., Wang, T., Zhou, X. Wu, W. and Wang, W. (2009). Measurement of aerosol number size distributions in the Yangtze River delta in China: Formation and growth of particles under polluted conditions. Atmos. Environ., 43, 829-836.
Guo, H., Ding, A., Morawska, L., He, C., Ayoko, G., Li,Y. and Hung, W. (2008). Size distribution and new particle formation in sub-tropical eastern Australia. Environmental Chemistry, 5, 382-390.
Harris, S.J. and Maricq, M.M. (2001). Signature size distributions for diesel and gasoline engine exhaust particulate matter. Journal of Aerosol Science, 32, 749-764.
Holman, J.P. (1972). Heat Transfer. New York, McGraw-Hill.
Holmes, N.S. (2007). A review of particle formation events and growth in the atmosphere in the various environments and discussion of mechanistic implications. Atmospheric Environment, 41, 2183-2201.
Hsu, S.-C., Lee, C.S.L., Huh, C.-A., Shaheen, R., Lin, F.-J. and Liu, S.C. (2014). Ammonium Deficiency Caused by Heterogeneous Reactions during a Super Asian Dust Episode. Journal of Geophysical Research, 119(11), doi:10.1002/2013JD021096.
Hughes, L.S., Cass, G.R., Gone, J., Ames, M. and Olmez, I. (1998). Physical and Chemical Characterization of Atmospheric Ultrafine Particles in the Los Angeles Area. Environmental Science and Technology, 32, 1153-1161.
Hussein, T., Dal Maso, M., Petäjä, T., Koponen, I.K., Paatero, P., Aalto, P.P., Hämeri, K. and Kulmala, M. (2005). Evaluation of an automatic algorithm for fitting the particle number size distributions. Boreal Env. Res. 10:337-355.
Juwono, A., Johnson, G.R., Mazaheri, M. and Morawska, L., Roux, F. and Kitchen, B. (2013). Investigation of the airborne submicrometer particles emitted by dredging vessels using a plume capture method. Atmospheric Environment, 73, 112-123.

Kulmala, M. (2003). How Particles Nucleate and Grow. Science, 302, 1000-1001.

Kulmala, M., Kontkanen, J., Junninen, H., Lehtipalo, K., Manninen, H.E., Nieminen, T., Petäjä, T., Sipilä, M., Schobesberger, S., Rantala, P., Franchin, A., Jokinen, T., Järvinen, E., Äijälä, M., Kangasluoma, J., Hakala, J., Aalto, P.P., Paasonen, P., Mikkilä, J., Vanhanen, J., Aalto, J., Hakola, H., Makkonen, U., Ruuskanen, T., Mauldin III, R.L., Duplissy, J., Vehkamäki, H., Bäck, J., Kortelainen, A., Riipinen I., Kurtén, T., Johnston, M.V., Smith, J.N., Ehn, M., Mentel, T.F., Lehtinen, K.E.J., Laaksonen, A., Kerminen, V.-M. and Worsnop, D.R. (2013). Direct Observations of Atmospheric Aerosol Nucleation. Science, 339, 943-946.

Kulmala, M., Petäjä, T., Nieminen, T., Sipilä, M., Manninen, H.E., Lehtipalo, K., Dal Maso, M., Aalto, P.P., Junninen, H., Paasonen, P., Riipinen, I., Lehtinen, K.E., Laaksonen, A. and Kerminen, V.-M. (2012). Measurement of the nucleation of atmospheric aerosol particles. Nature Protocols, 7, 1651-1667.

Kulmala, M., Vehkamäki, H., Petäjä, T., Dal Maso, M., Lauri, A., Kerminen, V.-M., Birmili, W. and McMurry, P.H. (2004). Formation and growth rates of ultrafine atmospheric particles: a review of observations. Journal of Aerosol Science, 35, 143-176.

Lehtinen, K.E.J., Dal Maso, M., Kulmala, M. and Kerminen, V.-M. (2007). Estimating nucleation rates from apparent particle formation rates and vice versa: Revised formulation of the Kerminen-Kulmala equation. J. Aerosol Sci., 38, 988-994, doi:10.1016/j.jaerosci.2007.06.009.

Li, C.-S. and Lin, C.-H. (2010). PM1/PM2.5/PM10 Characteristics in the Urban Atmosphere of Taipei. Aerosol Science and Technology, 36:4, 469-473.

Lin, C.-Y., Liu, S.C., Chou, C.C.-K., Liu, T.H. and Lee, C.-T. (2004). Long-Range Transport of Asian Dust and Air Pollutants to Taiwan. Terr. Atmos. and Ocean. Sci., 15, 759-784.

Lin, C.-Y., Chou, C. C.-K., Wang, Z., Lung, S.-C., Lee, C.-T., Yuan, C.-S., Chen, W.-N., Chang, S.-Y., Hsu, S.-C., Chen, W.-C. and Liu, S. C. (2012). Impact of different transport mechanisms of Asian dust and anthropogenic pollutants to Taiwan. Atmos. Environ., 60, 403-418.

Lundgren, D.A. Hlaing, D.N., Rich, T.A. and Marlpe, V.A. (1996). $PM_{10}/PM_{2.5}/PM_1$ Data from a Trichotomous Sampler. Aerosol Science and Technology, 25, 353-357.

Marple , V. A., Rubow, K. L. and Behm, S. M. (1991). A Microorifice Uniform Deposit Impactor (MOUDI): Description, Calibration, and Use, Aerosol Science and Technology, 14:4, 434-446.

Matsumoto, K., Uyama, Y., Hayano, T., Tanimoto, H., Uno, Itsushi. and Uematsu, M. (2003). Chemical properties and outflow patterns of anthropogenic and dust particles on Rishiri Island during the Asian Pacific Regional Aerosol

733 Characterization Experiment (ACE-Asia). Journal of Geophysical Research, 108
734 (D23), 8666, doi:10.1029/2003JD003426.
735 Mazaheri, M., Johnson, G.R. and Morawska, L. (2009). Particle and Gaseous
736 Emissions from Commercial Aircraft at Each Stage of the Landing and Takeoff
737 Cycle. Environmental Science and Technology, 43, 441-446.
738 Morawska, L., Ristovski, Z., Jayaratne, E.R., Keogh, D.U. and Ling, X. (2008).
739 Ambient nano and ultrafine particles from motor vehicle emissions: Characteristics,
740 ambient processing and implications on human exposure. Atmospheric Environment,
741 42, 8113-8138.
742 Nam, E., Kishan, S., Baldauf, R.W., Fulper, C.R., Sabisch, M. and Warila, J. (2010).
743 Temperature Effects on Particulate Matter Emissions from Light-Duty,
744 Gasonline-Powered Motor Vehicles. Environmental Science and Technology, 44,
745 4672-4677.
746 Nie, W., Ding, A., Wang, T., Kerminen, V.-M., George, C., Xue, L., Wang, W., Zhang,
747 Q., Petäjä, T., Qi, X., Gao, Xiaomei, Wang, X., Yang, X., Fu, C. and Kulmala.
748 (2014). Polluted dust promotes new particle formation and growth. Scientific
749 Reports, 4, 6634.
750 Pakkanen, T.A., Kerminen, V.-M., Korhonen, C.H., Hillamo, R.E., Aarnio, P.,
751 Koskentalo, T. and Maenhaut, W. (2001). Urban and rural ultrafine ($PM_{0.1}$) particles
752 in the Helsinki area. Atmospheric Environment, 35, 4593-4607.
753 Pérez, N., Pey, J., Cusack, M., Reche, C., Querol, X., Alastuey, A. and Viana, M
754 (2010). Variability of Particle Number, Black Carbon, and PM10, PM2.5 and PM1
755 Levels and Speciation: Influence of Road Traffic Emissions on Urban Air Quality.
756 Aerosol Science and Technology, 44, 487-499.
757 Petäjä, T., Mauldin III, R.L., Kosciuch, E., McGrath, J., Nieminen, T., Paasonen, P.,
758 Boy, M., Adamov, A., Kotiaho, T. and Kulmala, M. (2009). Sulfuric acid and OH
759 concentrations in a boreal forest site. Atmospheric Chemistry and Physics, 9,
760 7435-7448.
761 Pey, J., Rodíguez, S., Querol, X., Alastuey, A., Moreno, T., Putaud, J.P., and Van
762 Dingenen, R (2008). Variations of urban aerosols in the western Mediterranean.
763 Atmospheric Environment, 42, 9052-9062.
764 Pey, J., Querol, X., Alastuey, A., Rodiguez, S., Putaud, J.P. and Van Dingenen, R.
765 (2009). Source apportionment of urban fine and ultrafine particle number
766 concentration in a Western Mediterranean city. Atmospheric Environment, 43,
767 4407-4415.
768 Reche, C., Querol, X., Alastuey, A., Viana, M., Pey, J., Moreno, T., Rodríguez, S.,
769 González, Y., Fernández-Camacho, R., de la Rosa, J., Dall'Osto, M., Prévôt, A.S.H.,
770 Hueglin, C., Harrison, R.M. and Quincey, P. (2011). New considerations for PM,

771 Black Carbon and particle number concentration for air quality monitoring across
772 different European cities. Atmospheric Chemistry and Physics, 11, 6207-6227, 2011.
773 Ristovski, Z.D., Jayaratne, E.R., Lim, M., Ayoko, G.A. and Morawska, L. (2006).
774 Influence of diesel fuel sulphur on the nanoparticle emissions from city buses.
775 Environmental Science and Technology, 40, 1314-1320.
776 Salvador, C.M. and Chou, C.C.-K. (2014). Analysis of semi-volatile materials (SVM)
777 in fine particulate matter. Atmospheric Environment, 95, 288-295.
778 Subramanian, R., Khlystov, A.Y., Cabada, J.C. and Robinson, A.L. (2004). Positive
779 and negative artifacts in particulate organic carbon measurements with denuded and
780 undenuded sampler configurations. Aerosol Science and Technology, 38, 27-48.
781 Turpin, B.J. and Lim, H.-J. (2001). Species contributions to PM2.5 mass
782 concentrations: revisiting common assumptions for estimating organic mass. Aerosol
783 Science and Technology, 35, 602-610.
784 Vallius, M.J. Ruuskanen, J. Mirme, A. and Pekkanen, J. (2000). Concentrations and
785 Estimated Soot Content of PM_1, $PM_{2.5}$ and PM_{10} in a Subarctic Urban Atmosphere.
786 Environmental Science and Technology, 34, 1919-1925.
787 Wang, T., Ding, A.J., Blake, D.R., Zahorowski, W., Poon, C.N. and Li, Y-S. (2003).
788 Chemical characterization of the boundary layer outflow of air pollution to Hong
789 Kong during February-April 2001.
790 Wang, D., Guo, H., Cheung, K. and Gan, F. (2014). Observation of nucleation mode
791 particle burst and new particle formation events at an urban site in Hong Kong.
792 Atmospheric Environment, 99, 196-205.
793 Wang Z. B., Hu, M., Suu, J.Y., Wu, Z.J., Yue, D.L., Shen, X.J., Zhang, Y.M., Pei, X.Y.,
794 Cheng, Y.F. and Wiedensohler, A. (2013). Characteristics of regional new particle
795 formation in urban and regional background environments in the North China Plain.
796 Atmospheric Chemistry and Physics, 13, 12495-12506.
797 Woo, K.S., Chen, D.R., Pui, D.Y.H. and McMurry, P.H. (2001). Measurement of
798 Atlanta aerosol size distribution: observation of ultrafine particle events. Aerosol
799 Science and Technology, 34, 75-87.
800 Wu Z., Hu, M., Lin, P., Liu, S., Wehner, B. and Wiedensohler, A. (2008). Particle
801 number size distribution in the urban atmosphere of Beijing, China. Atmospheric
802 Environment, 42, 7967-7980.
803

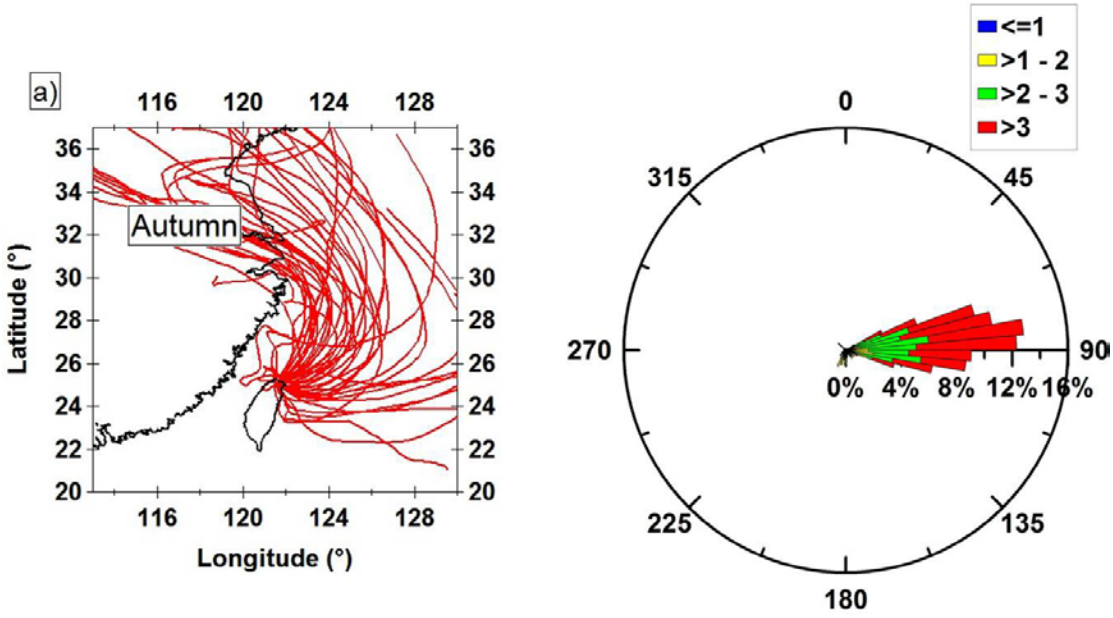
a)
Autumn
Latitude (°)
Longitude (°)
116
120
124
128
20
22
24
26
28
30
32
34
36
<=1
>1 - 2
>2 - 3
>3
0
45
90
135
180
225
270
315
0%
4%
8%
12%
16%

804

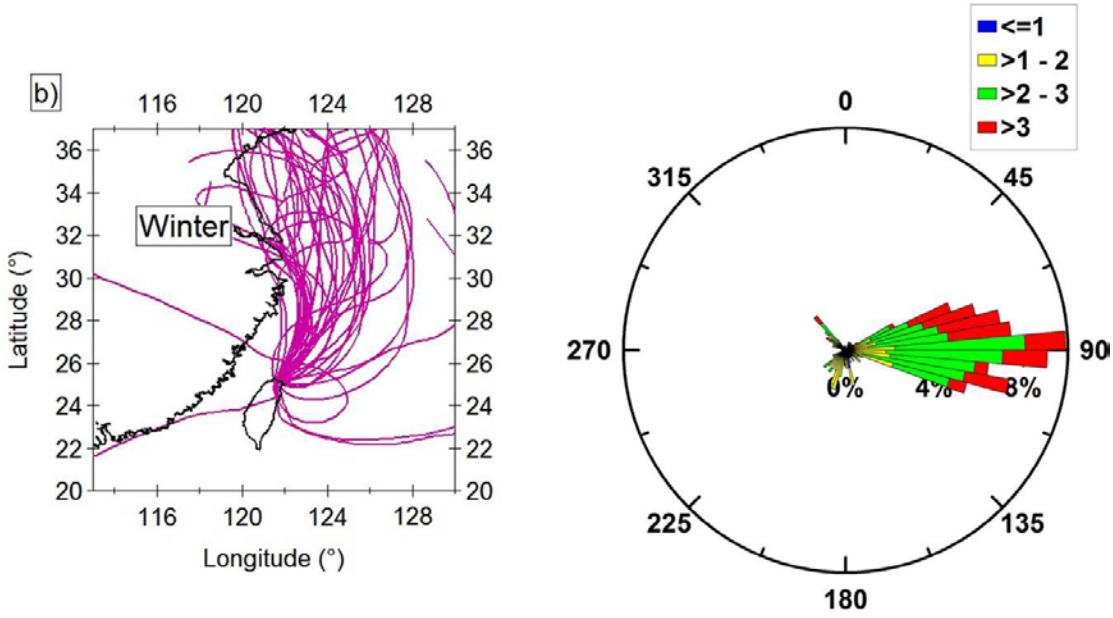
b)
Winter
Latitude (°)
Longitude (°)
116
120
124
128
20
22
24
26
28
30
32
34
36
<=1
>1 - 2
>2 - 3
>3
0
45
90
135
180
225
270
315
0%
4%
8%

805

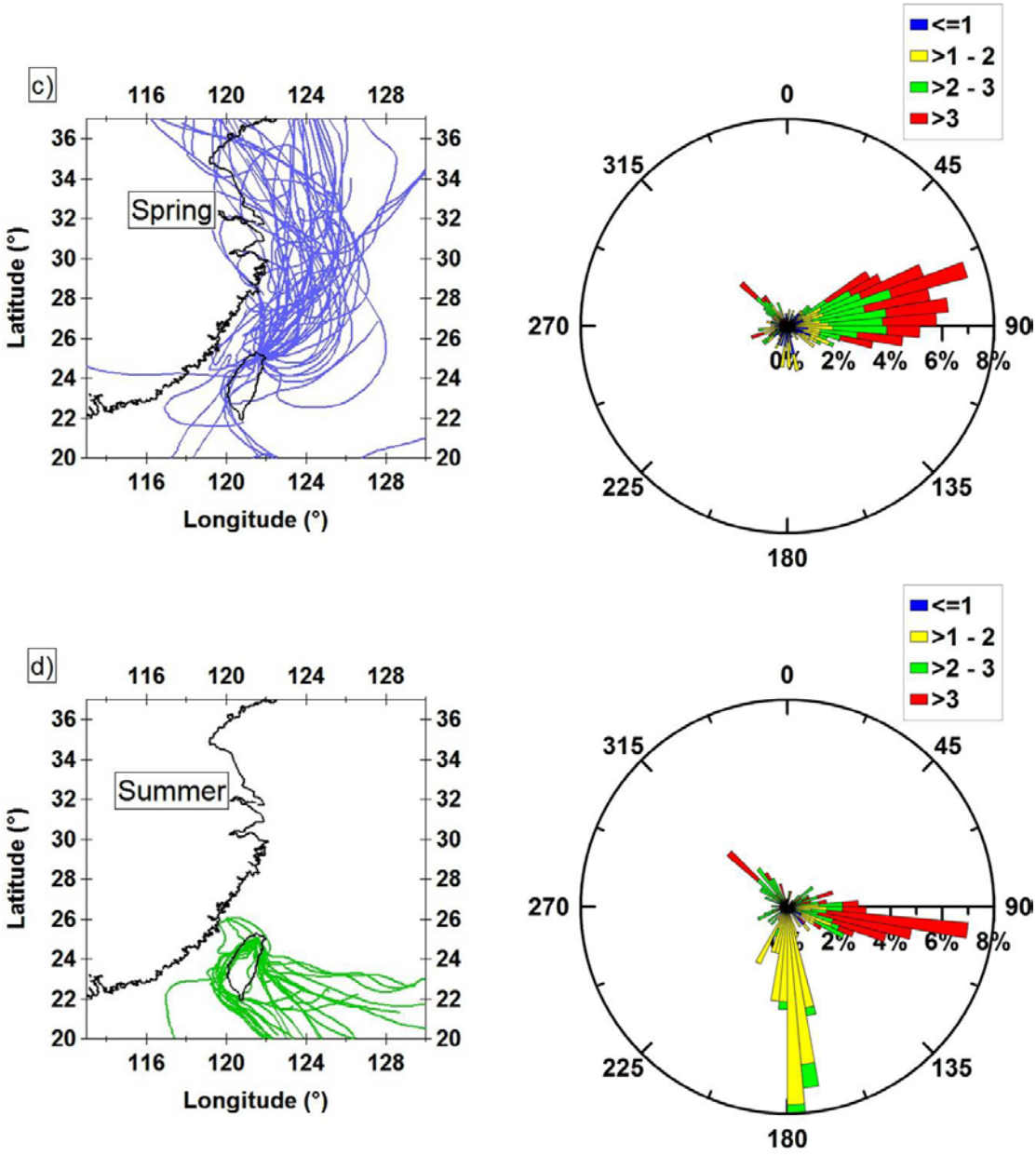

806

807

808

809 **Figure 1**. Back-trajectories calculated for TARO for the measurement periods (left panel) and
810 surface wind rose plots (right panel) in **(a)** autumn, **(b)** winter, **(c)** spring and **(d)** summer. The
811 color codes of wind rose plots represent the wind speed: blue < 1 ms^{-1}; yellow 1-2 ms^{-1}; green
812 2-3 ms^{-1}; and red > 3 ms^{-1}.

813

814

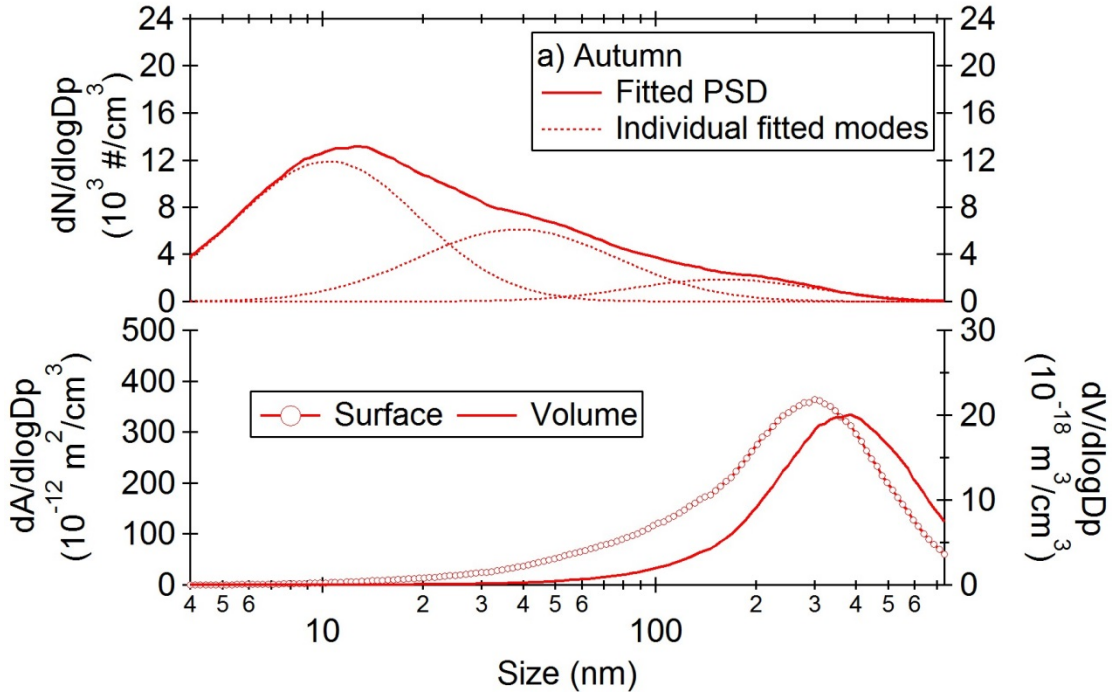
a) Autumn
Fitted PSD
Individual fitted modes
dN/dlogDp (10^3 #/cm^3)
dA/dlogDp (10^-12 m^2/cm^3)
dV/dlogDp (10^-18 m^3/cm^3)
Surface
Volume
Size (nm)

815

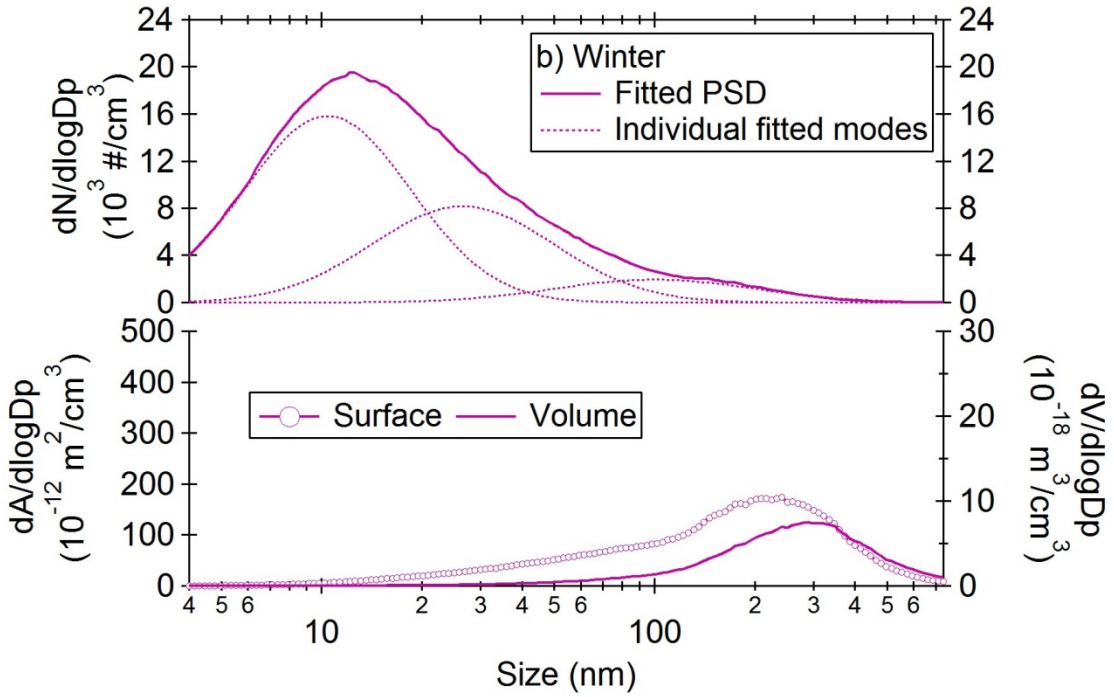
b) Winter
Fitted PSD
Individual fitted modes
dN/dlogDp (10^3 #/cm^3)
dA/dlogDp (10^-12 m^2/cm^3)
dV/dlogDp (10^-18 m^3/cm^3)
Surface
Volume
Size (nm)

816

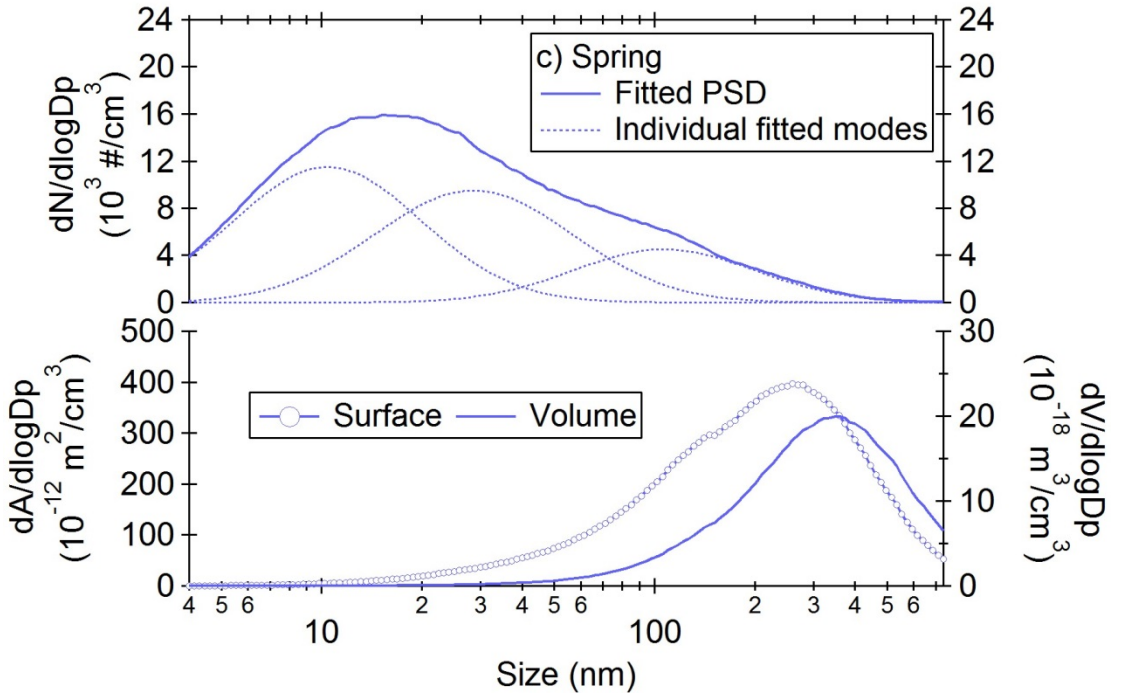

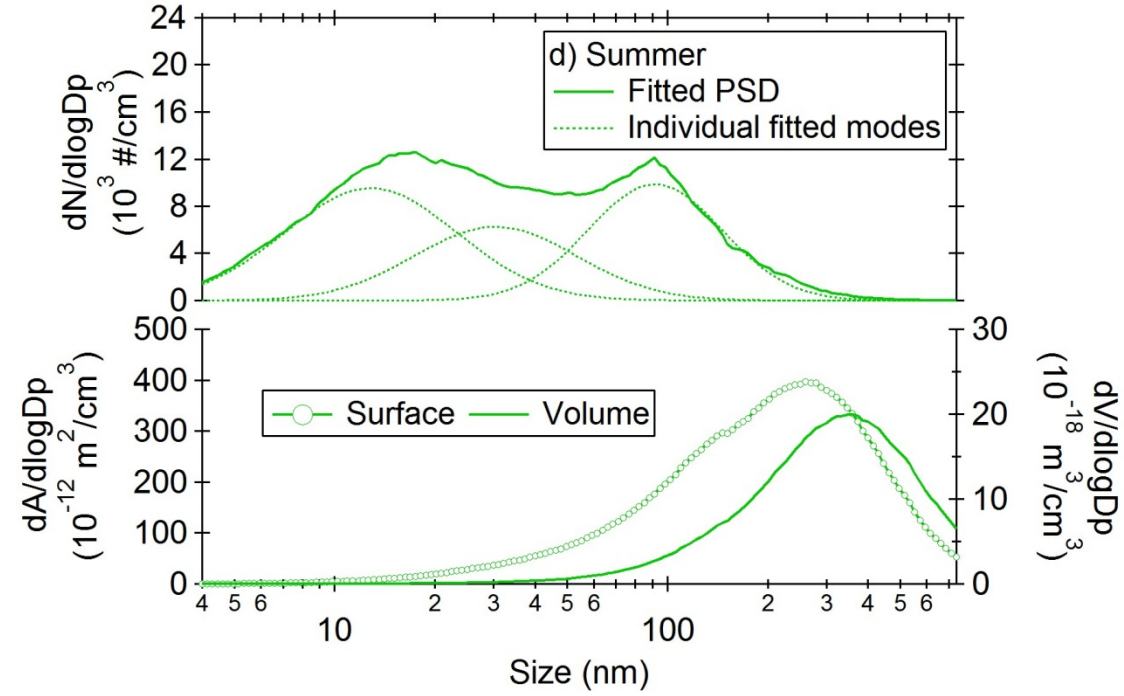

Figure 2. Size distribution of particle number (upper panel), surface and volume (lower panel) concentrations measured in **(a)** autumn, **(b)** winter, **(c)** spring and **(d)** summer (by curve fitting).

Figure 3. Seasonal average concentration and composition of **(a)** ultra-fine (UFPs) and **(b)** sub-micron (PM_1) particles observed at the TARO in Taipei, Taiwan from autumn 2012 to summer 2013.

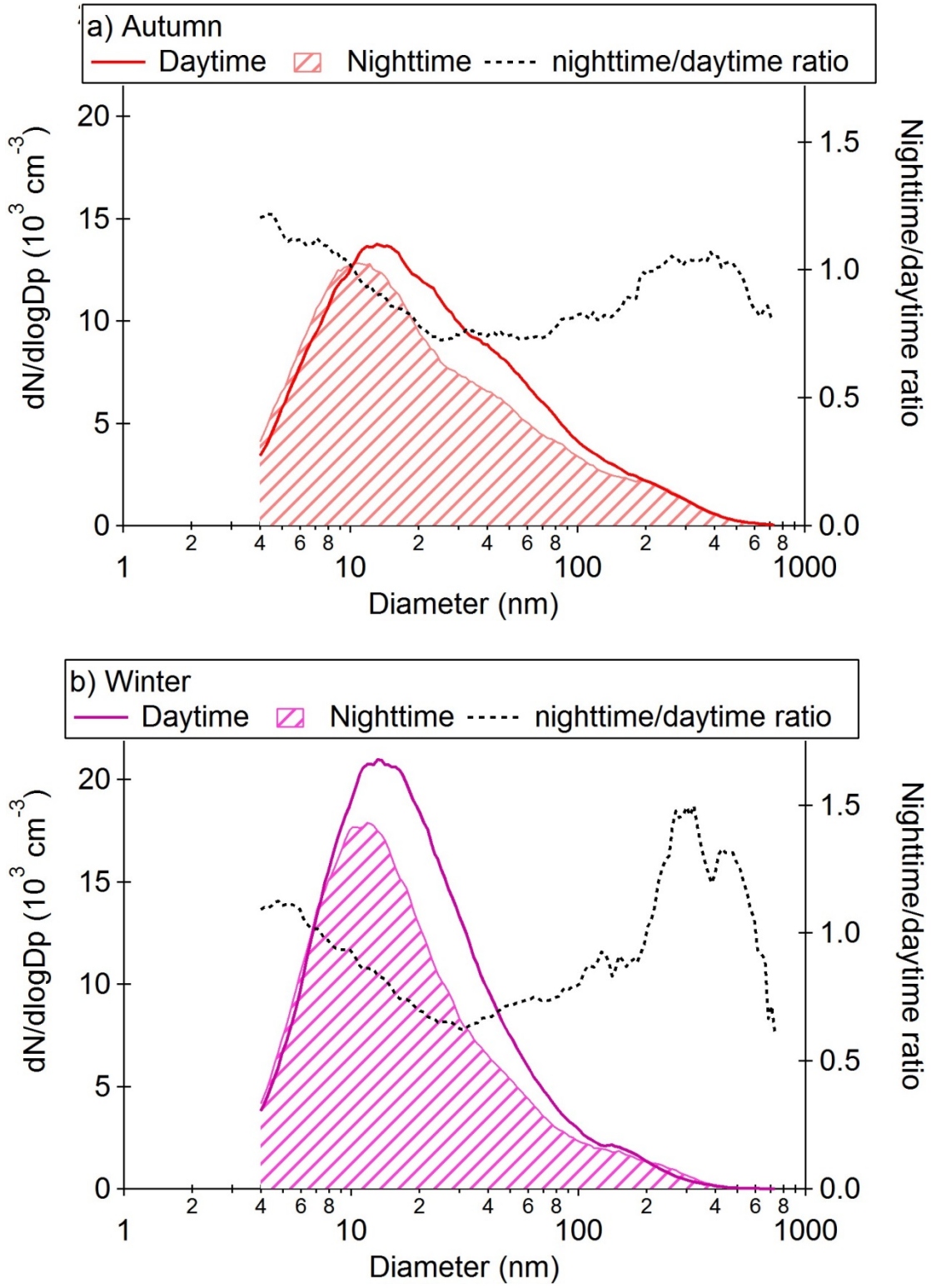
a) Autumn
Daytime
Nighttime
nighttime/daytime ratio
dN/dlogDp (10^3 cm^-3)
Nighttime/daytime ratio
Diameter (nm)
b) Winter
Daytime
Nighttime
nighttime/daytime ratio
dN/dlogDp (10^3 cm^-3)
Nighttime/daytime ratio
Diameter (nm)

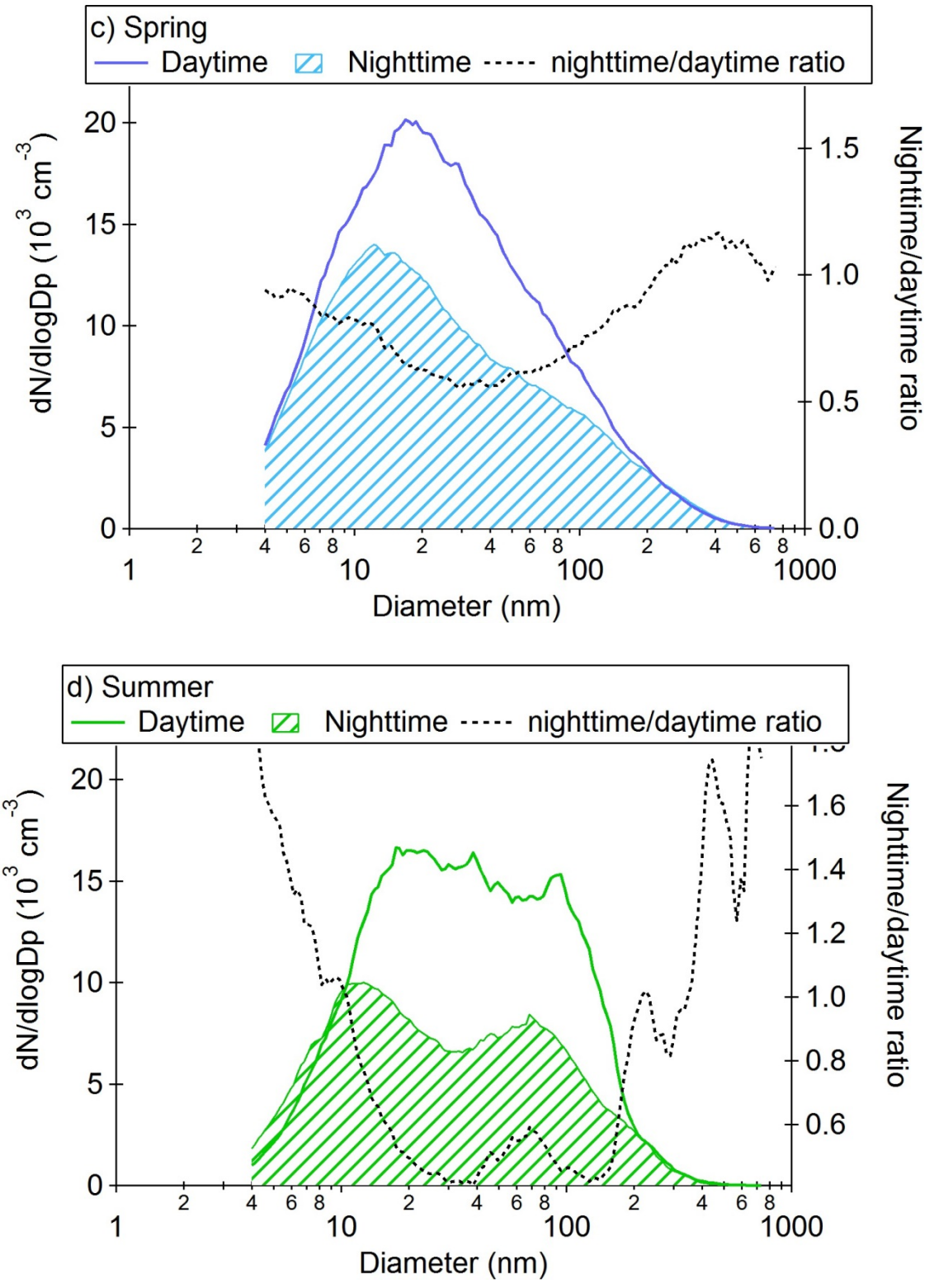

Figure 4. Median PSDs measured during the daytime (07:00 – 17:00 LT) and nighttime (17:00 – 07:00) in **(a)** autumn, **(b)** winter, **(c)** spring and **(d)** summer.

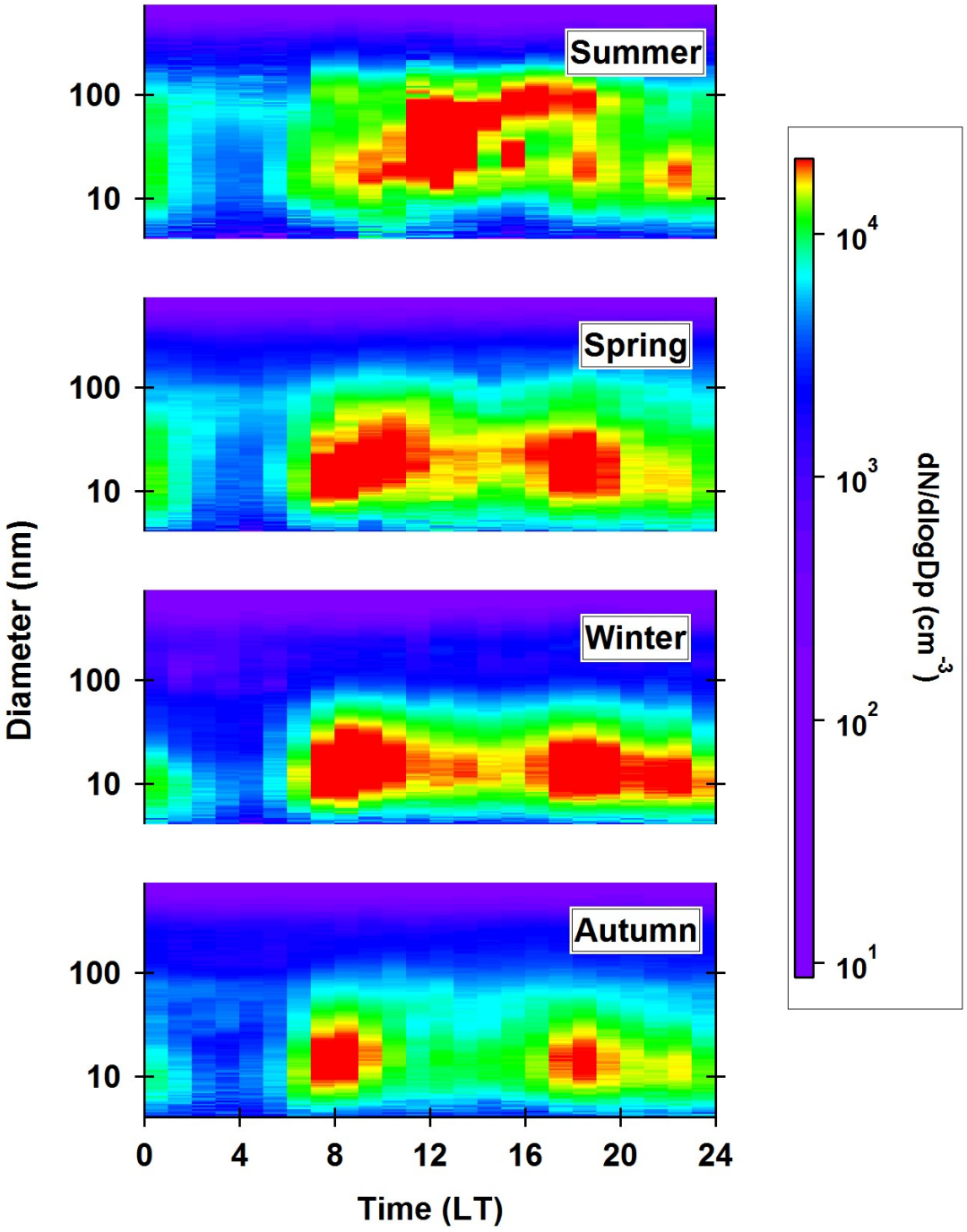

849
850
851 **Figure 5.** Diurnal variation of particle number size distribution in each season. From lower
852 panel to top panel: autumn, winter, spring and summer.
853
854

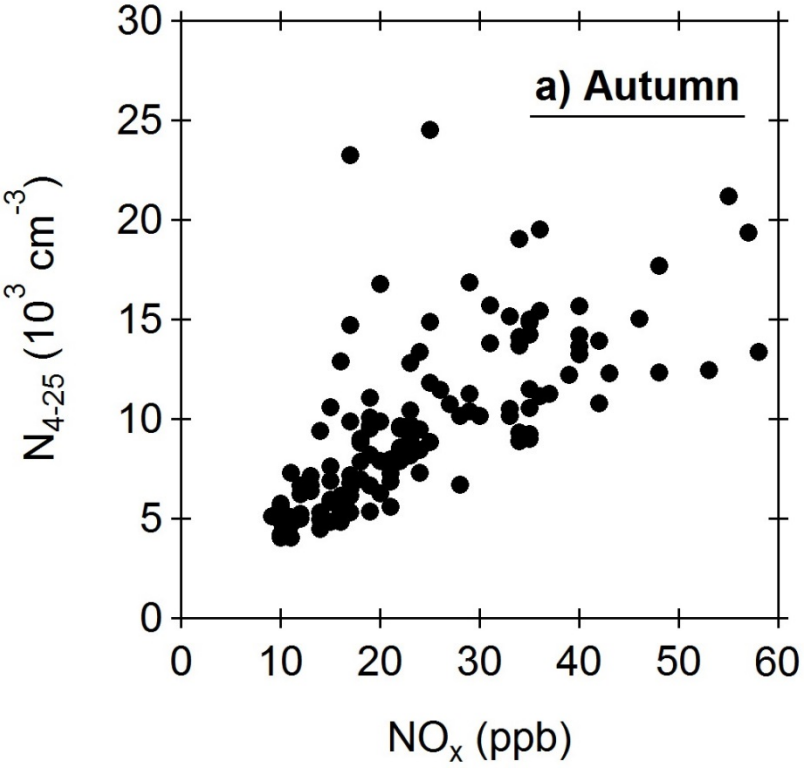

880

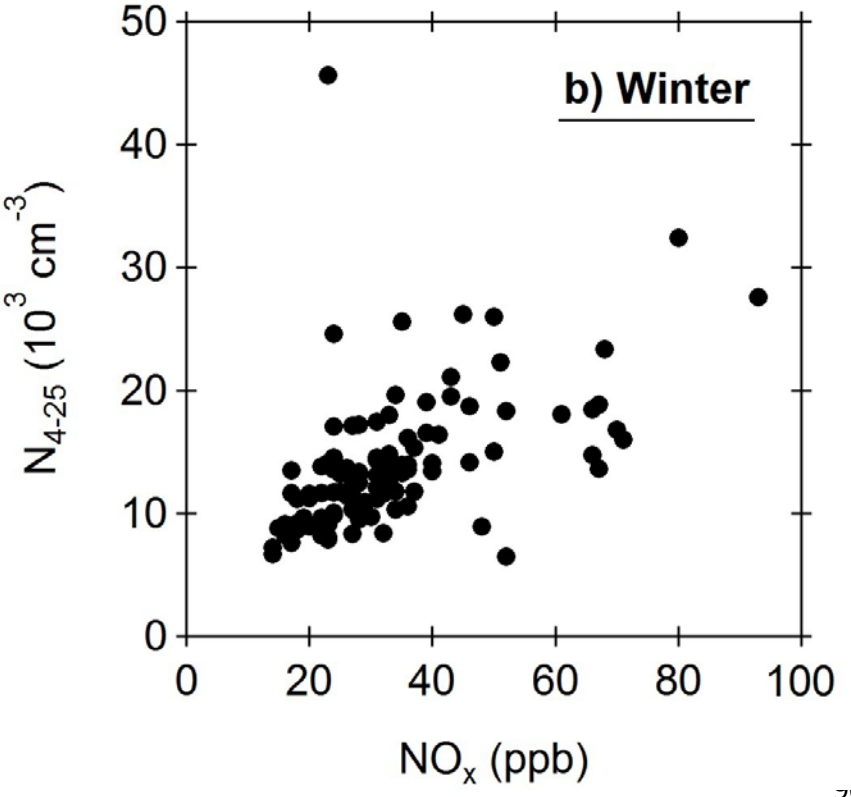

900

907
908
909
910
911

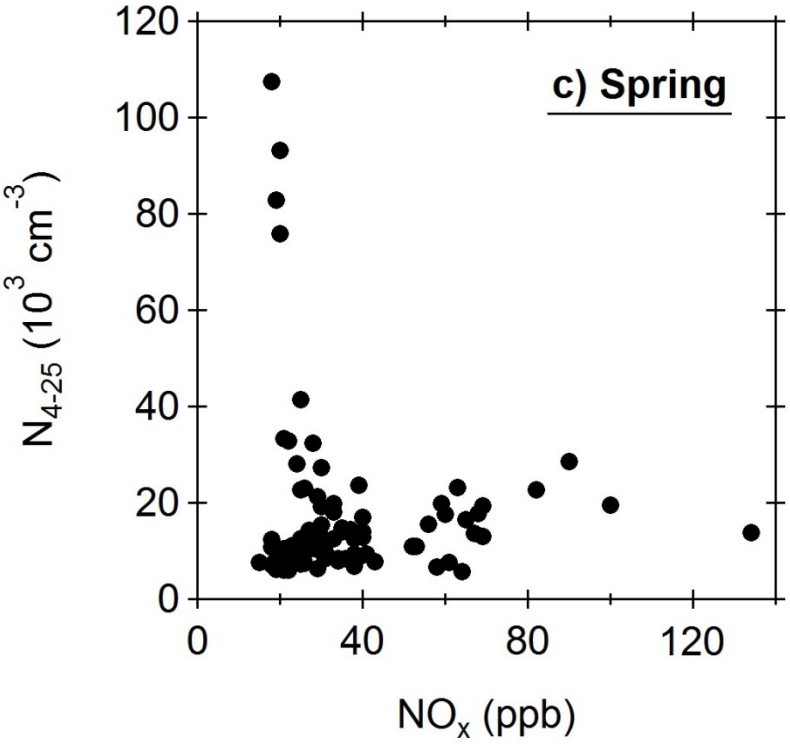

936

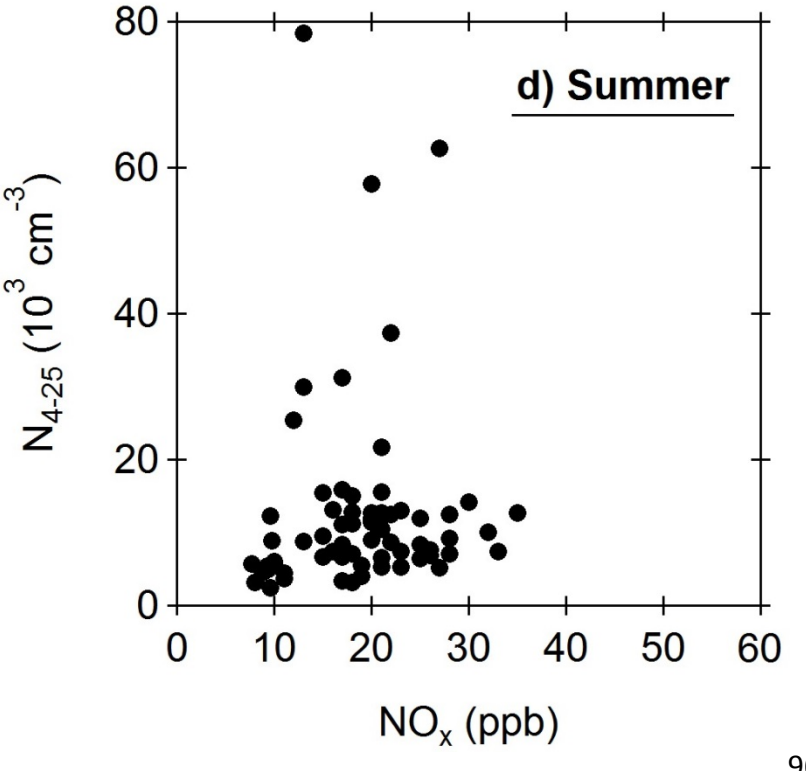

961

962 **Figure 6**. Scatter plots between hourly $N_{4\text{-}25}$ and NO_x observed in **(a)** Autumn, **(b)** Winter, **(c)**
963 Spring and **(d)** Summer at TARO site during the period of 07:00 – 17:00 LT.

964

965

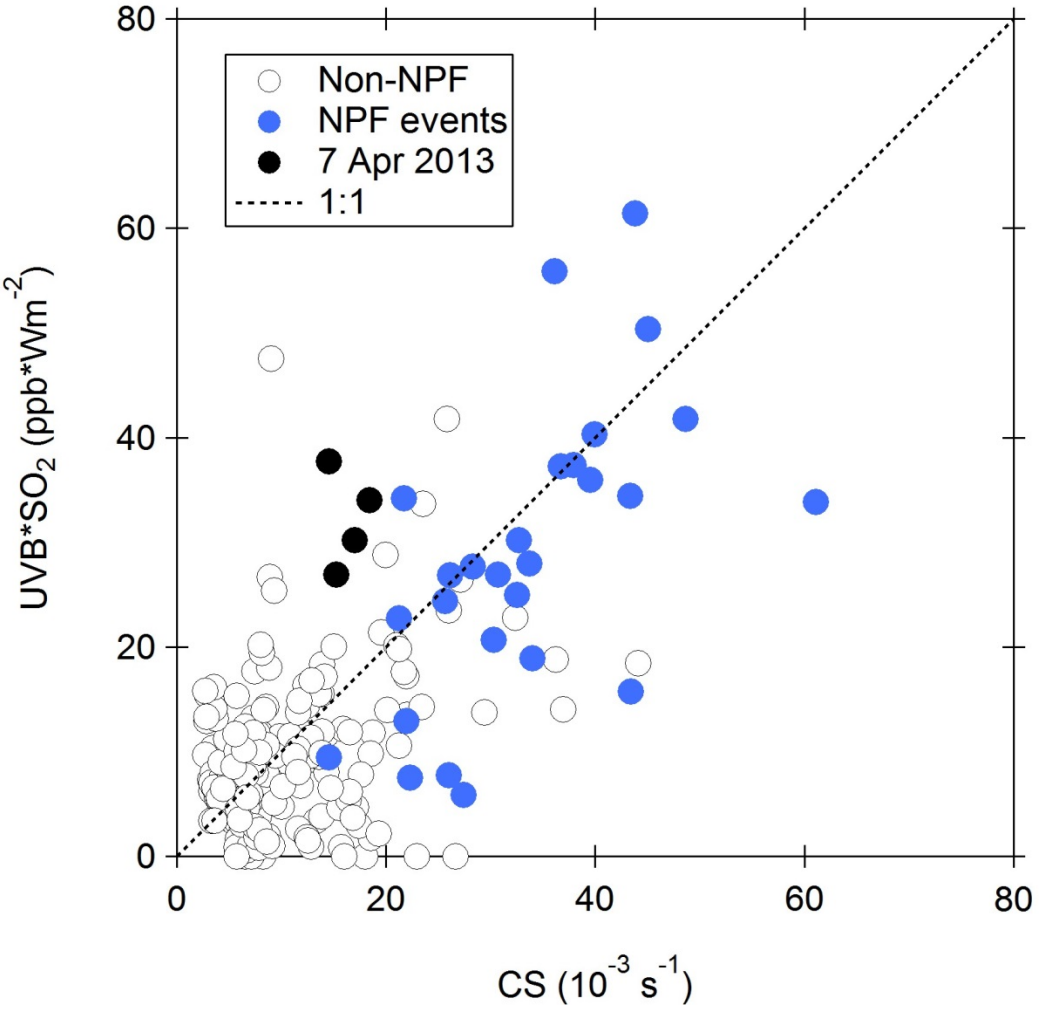

966

967

968 **Figure 7.** Scatter plot of hourly averaged UVB*SO_2 versus condensation sink at noontime

969 (10:00 – 14:00 LT).

970

971

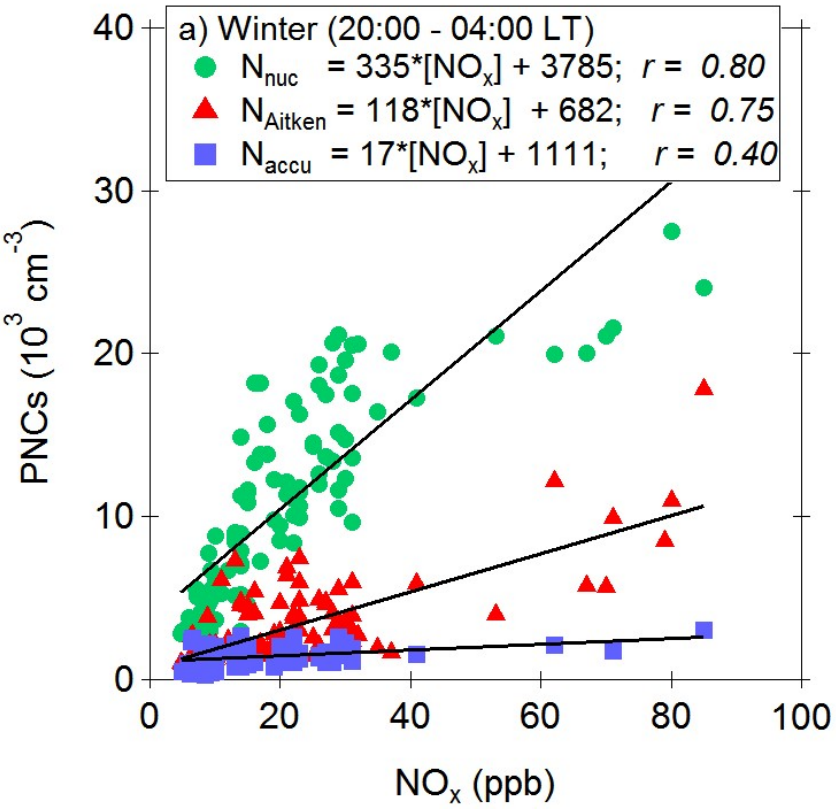

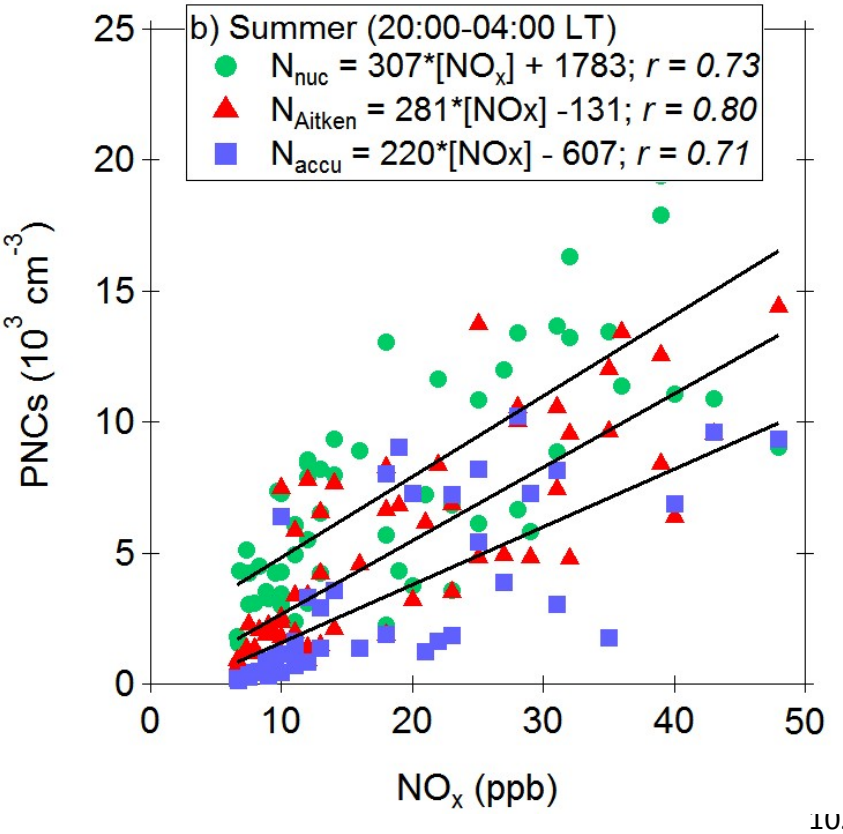

Figure 8. Scatter plots for hourly averaged PNCs vs. NO_x measured during the time period of 20:00 – 04:00 (LT) in **(a)** winter and **(b)** summer, with classification of various particle size ranges.

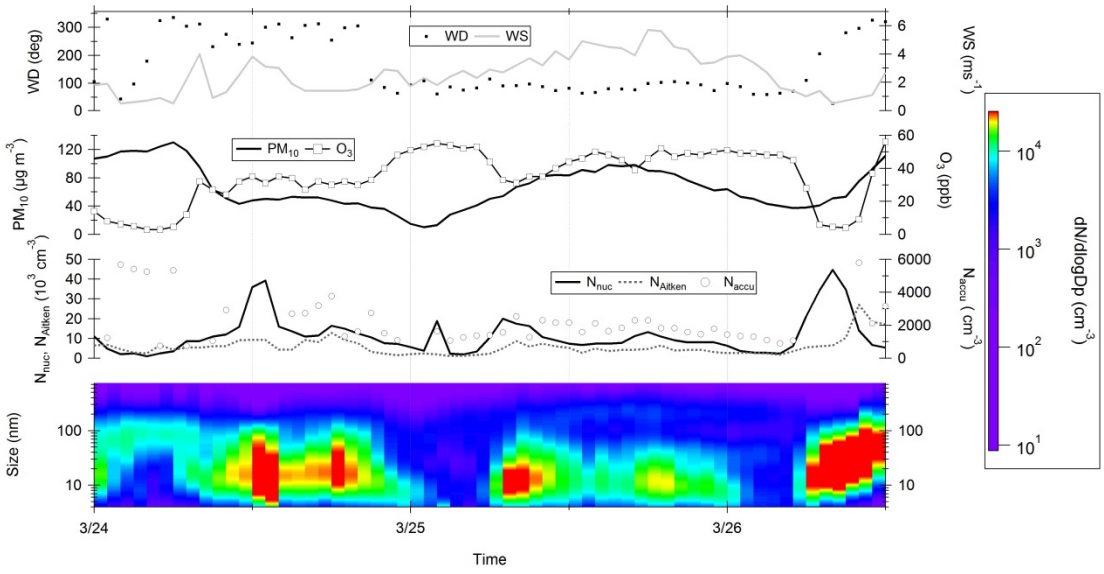

Figure 9. Time series of PSD, the $N_{4\text{-}25}$, $N_{25\text{-}100}$, $N_{100\text{-}736}$, PM_{10}, ozone (O_3) and wind direction/speed measured from 24 - 26 March 2013 (from bottom to top).

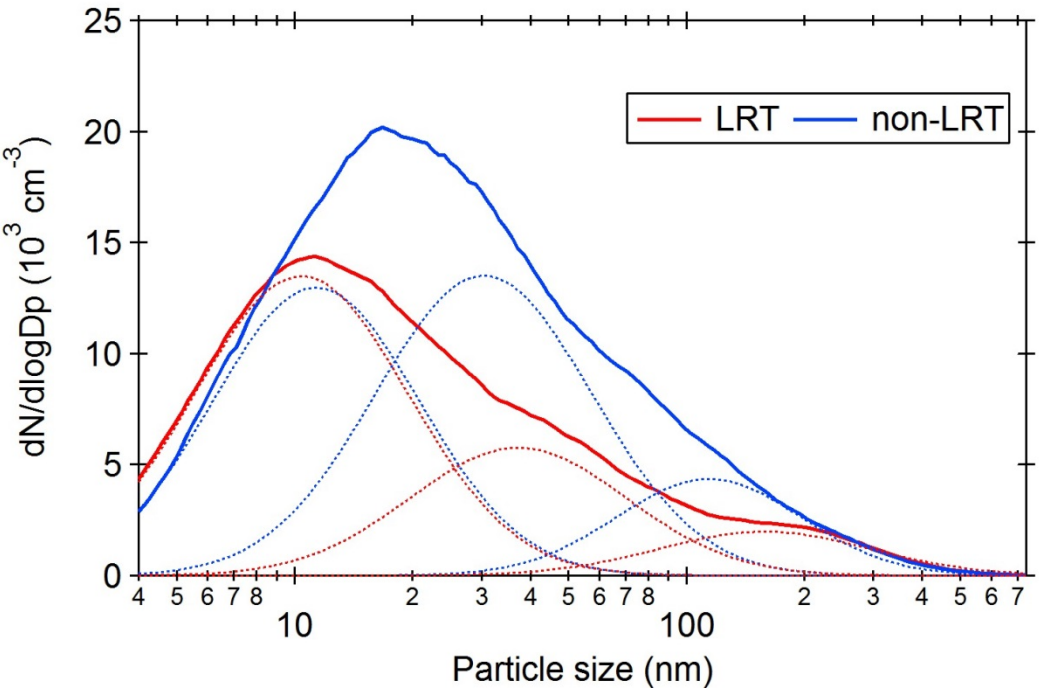

Figure 10. Averaged PSDs for LRT and non-LRT episodes measured during the seasons of winter monsoons. Dashed lines illustrate the PSD of each individual mode.